

W. Tian, T. A. Sevilla, W. Zuo, M. D. Sohn 2017. “Coupling Fast Fluid Dynamics and Multizone Airflow Models in Modelica Buildings Library to Simulate the Dynamics of HVAC Systems.” *Building and Environment*, 122, pp. 269-286. DOI: 10.1016/j.buildenv.2017.06.013.

Coupling Fast Fluid Dynamics and Multizone Airflow Models in Modelica *Buildings* Library to Simulate the Dynamics of HVAC Systems

Wei Tian^a, Thomas Alonso Sevilla^a, Wangda Zuo^{a*}, Michael D. Sohn^b

^a *Department of Civil, Architectural and Environmental Engineering, University of Miami, 1251 Memorial Drive, Coral Gables, FL 33146, U.S.A.*

^b *Energy Analysis and Environmental Impacts Division, Lawrence Berkeley National Laboratory, 1 Cyclotron Road, Berkeley, CA 94720, U.S.A.*

Abstract

Multizone models are widely used in building airflow and energy performance simulations due to their fast computing speed. However, multizone models assume that the air in a room is well mixed, consequently limiting their application. In specific rooms where this assumption fails, the use of computational fluid dynamics (CFD) models may be an alternative option. Previous research has mainly focused on coupling CFD models and multizone models to study airflow in large spaces. While significant, most of these analyses did not consider the coupled simulation of the building airflow with the building's Heating, Ventilation, and Air-Conditioning (HVAC) systems. This paper tries to fill the gap by integrating the models for HVAC systems with coupled multizone and CFD simulations for airflows, using the Modelica simulation platform. To improve the computational efficiency, we incorporated a simplified CFD model named fast fluid dynamics (FFD). We first introduce the data synchronization strategy and implementation in Modelica. Then, we verify the implementation using two case studies involving an isothermal and a non-isothermal flow by comparing model simulations to experiment data. Afterward, we study another three cases that are deemed more realistic. This is done by attaching a variable air volume (VAV) terminal box and a VAV system to previous flows to assess the capability of the models in studying the dynamic

* Corresponding author: w.zuo@miami.edu

control of HVAC systems. Finally, we discuss further research needs on the coupled simulation using the models.

Key words: Fast Fluid Dynamics, Multizone Airflow Networks, Modelica, HVAC Modeling

1 Introduction

In order to make Heating, Ventilation, and Air-Conditioning (HVAC) systems operate efficiently during a building's life cycle, it is necessary to carry out building performance simulations to verify and improve the system design (Clarke 2001; Nguyen et al. 2014). Usually, in a simulation program, the HVAC model and indoor airflow model are coupled to mutually exchange information to assess the building as a whole (Tian and Zuo 2013). In a conventional building performance simulation program such as EnergyPlus (Crawley et al. 2000), the multizone airflow models (Axley 2007) are initially implemented to save computing time for the simulation of a building's annual energy performance. However, for buildings with stratified airflow distribution, the assumption of the multizone models (Wang and Chen 2008) fails, and researchers (Beausoleil-Morrison 2000; Zhai et al. 2002) proposed solutions to substitute the multizone models with computational fluid dynamics (CFD) (Ladeinde and Nearon 1997) models. While solving the problem, it significantly increased the computing time especially for large spaces.

To provide a timely prediction of airflow in large buildings consisting of multiple zones, or rooms, researchers proposed to apply only the CFD model to a few zones with stratified airflow while also utilizing the multizone models for the rest of the building. Gao (2002) developed methodologies to couple CONTAM (Walton 1994) with a CFD program called MIT-CFD. Three different data synchronization strategies (virtual coupling, quasi-dynamics coupling, and dynamic coupling) were proposed. Case studies had been carried out to use the developed model to study common indoor airflow types such as forced convection, natural convection and contaminant transportation in a building (Yuan 2003; Tan and Glicksman 2005). Wang and Chen (2007) further validated the dynamic coupling

strategy by using experiments in which stratified airflows were involved including the non-uniform distribution of momentum, temperature, and contaminant (Wang and Chen 2007; Srebric et al. 2008).

While significant, previous work focused strictly on the airflow movement and left out modeling of HVAC systems and controls. It is critical to add the HVAC modeling of the coupled multizone and CFD models for airflow to seek a holistic solution for building ventilation control. There are many existing HVAC modeling proposals, such as EnergyPlus (Crawley et al. 2000), DOE-2 (Birdsall et al. 1985) and Modelica-based models (Fritzon 1998). On one hand, some programs were designed for whole-year energy simulation and used quasi-steady models to approximate the dynamic process. For example, EnergyPlus adopts an ideal PI control which cannot simulate overshoot or error band which exists in a real HVAC system. EnergyPlus also ignores the dead band and waiting time which are critical for system control. Nevertheless, some programs can model the dynamic process to a certain level, but capturing all the dynamic response increases the computational cost. For example, TRNSYS (Klein et al. 1976) is designed to model the dynamic behavior of HVAC systems but with a fixed time step size. In order to capture the complete dynamics, the time step size needs to be set small enough (Wetter and Haugstetter 2006b). Yet, using a small time step size results in lengthy computing time for the entire simulation.

To support dynamic modeling and simulation of HVAC systems in an efficient way, Lawrence Berkeley National Laboratory (Wetter et al. 2014; Wetter et al. 2015) developed the *Buildings* library consisting of room airflow, HVAC, control and building envelope models for use in building energy and control system simulation. The *Buildings* library is

implemented using Modelica, an equation-based and object-oriented modeling language. Besides the multizone models, there are several CFD model implementations in Modelica such as a sub-zonal CFD model (Bonvini et al. 2014) and VEPZO (Norrefeldt et al. 2012). Note that multizone models similar to CONTAM (Walton 1994) are also included in the *Buildings* library (Wetter 2006). Similarly, the Modelica environment can support an adaptive time step size to capture all the dynamics while maintaining optimal computational efficiency. Previous work based on the *Buildings* library, created a coupled simulation that allowed for the dynamic interaction between the stratified airflow, HVAC, control and building envelope models (Zuo et al. 2014; Zuo et al. 2016). In that work, a fast fluid dynamics (FFD) model (Zuo and Chen 2009) was used to simulate the stratified airflow distribution within a room. However, in the work of Zuo et al. (Zuo et al. 2014; Zuo et al. 2016), FFD used a constant pressure that was independent of the pressure of the Modelica model. Instead of calculating the mass flow rate according to the pressure difference between two rooms, the FFD used in the *Room.CFD* model (a room heat and mass balance model that uses CFD to predict airflow distribution) must rely on Modelica to provide the inlet mass flow rate. As a result, the model can only be used as a standalone tool, and cannot be linked to the multizone models in the library to simulate the airflow distribution within a large building. Similarly, it is not feasible to connect *Room.CFD* and *Room.MixedAir* which is a room heat and mass balance model that assumes the air in the room is well-mixed (Nouidui, Wetter, et al. 2012; Nouidui, Phalak, et al. 2012), for the study of the thermal environment, envelopes and system control in a building that typically contains many rooms.

To integrate the coupled airflow simulation of CFD-multizone with the models for HVAC and control, this paper reports our research in the coupling of three models based on the Modelica *Buildings* library and CFD. Although the coupling scheme can employ any CFD program, this paper uses FFD as an example since it is about 50 times faster than CFD (Zuo and Chen 2009). For ease of writing, in the rest of the paper, we use FFD only, whereas the reader should bear in mind that FFD can be replaced by conventional CFD programs. We first introduce the implementation of data synchronization between FFD and multizone models. Then we verify the implementation using two case studies involving an isothermal flow and a non-isothermal flow and compare the results with experimental data. Afterward, we study another three cases with more complicated/realistic building configurations. Finally, we discuss further research needs on the coupled simulation model.

2 Research Methodology

2.1 Mathematical Description of FFD and Multizone Models

2.1.1 FFD Model

FFD solves the Navier-Stokes equations:

$$\frac{\partial \mathbf{U}_i}{\partial t} = -\mathbf{U}_j \frac{\partial \mathbf{U}_i}{\partial x_j} + \nu \frac{\partial^2 \mathbf{U}_i}{\partial x_j \partial x_j} - \frac{1}{\rho} \frac{\partial P}{\partial x_i} + \mathbf{F}_i \quad (1)$$

where \mathbf{U}_i and \mathbf{U}_j are the velocity component in x_i and x_j directions, respectively, ν is the kinematic viscosity, ρ is the fluid density, P is the pressure, t is the time, and \mathbf{F}_i is the source term, such as the buoyancy force. FFD splits the Navier-Stokes equation into the following three equations:

$$\frac{\partial \mathbf{U}_i}{\partial t} = -\mathbf{U}_j \frac{\partial \mathbf{U}_i}{\partial x_j} \quad (2)$$

$$\frac{\partial \mathbf{U}_i}{\partial t} = \nu \frac{\partial^2 \mathbf{U}_i}{\partial x_j^2} + \mathbf{F}_i \quad (3)$$

$$\frac{\partial \mathbf{U}_i}{\partial t} = -\frac{1}{\rho} \frac{\partial P}{\partial x_i} \quad (4)$$

FFD first solves the advection equation (2) using a semi-Lagrangian method (Courant et al. 1952). It then solves the diffusion equation (3) with an implicit scheme. Finally, it solves the pressure equation (4) together with the continuity equation

$$\frac{\partial \mathbf{U}_i}{\partial x_i} = 0 \quad (5)$$

using a projection-correction method (Chorin 1967). FFD applies a similar algorithm to solve the conservation equations of energy and species. In the literature, both the sequential FFD programs (Zuo and Chen 2009; Jin et al. 2012) and parallel FFD programs (Zuo and Chen 2010; Yang 2013; Tian, Sevilla, and Zuo 2017) are available.

2.1.2 Multizone Model

A typical multizone model uses a power law relation to express flow as a function through an orifice. In the power law equation, the mass flow rate \dot{m}_{ij} represents the flow from zone i to zone j (Dols and Walton 2002):

$$\dot{m}_{ij} = C_d A \sqrt{2\rho \Delta P}^m \quad (6)$$

where C_d is the discharge coefficient normally ranging between 0.6 to 0.75; A is the area size of the opening; ρ is the density of the air; m is constant, which is 0.5 for large openings. ΔP is the pressure difference which is the aggregate sum of the total pressure difference $|P_i - P_j|$, and pressure difference as a result of wind ΔP_w , and pressure difference due to density and elevation difference ΔP_t (Wang and Chen 2007).

Since Modelica is an equation-based, object-oriented modeling language (Fritzson 1998), the sign of \dot{m}_{ij} can be automatically determined based on the pressure in two zones. Thus, we can write the mass conservation for zone i as:

$$\frac{dm_i}{dt} = \sum_{j=1}^n \dot{m}_{ij} + F_i \quad (7)$$

where t is time; n is number of surrounding neighbors to zone j ; m_i is the air mass in the zone i ; F_i is the air mass source in the zone i . Once the boundary conditions (e.g. ambient pressure) are applied, the pressure at each zone and mass flow rate between neighboring zones can be determined uniquely.

2.2 Coupling Strategies between FFD and Multizone Model

As defined by Zhai et al. (2002), there are mainly three categories in coupling two building simulation programs: static coupling, dynamic coupling, and quasi-dynamic coupling.

Considering that we would need to couple the HVAC and control simulation later, we chose the quasi-dynamic coupling strategy (Figure 1) which provides a suitable balance between computing time and capturing system dynamics. A quasi-dynamic coupling requires that FFD and multizone models exchange information consisting of

$\mathbf{x}_1(t_n)$ and $\mathbf{x}_2(t_n)$ mutually at data synchronization time points t_n . After data synchronization is completed, the two programs will run separately for one synchronization time step Δt_{syn} until the next data synchronization point. FFD uses a constant time step size Δt_{ffd} while the multizone model, implemented in Modelica, adopts a variable time step size that is automatically determined in the implicit integration algorithm to solve the equations efficiently (Wetter and Haugstetter 2006a). The synchronization time step size Δt_{syn} is a constant set by the user. It should be a multiple of Δt_{ffd} to ensure the FFD

simulation completes its time advance step when it starts to synchronize the data. On the Modelica side, we used a “sample” function to forcibly execute a data exchange at a period of Δt_{syn} .

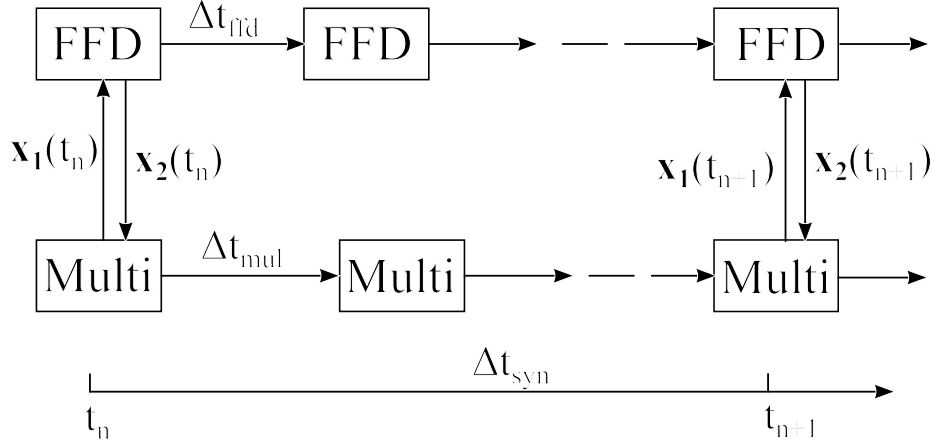


Figure 1 Quasi-dynamic coupling between FFD and multizone model

The exchanged data x_1 and x_2 between the two programs can vary according to boundary conditions applied to FFD. If the inlet flow rate for FFD is known prior to multizone model calculation, the velocity boundary condition is applied to FFD. Otherwise, the pressure boundary condition is applied. In the following sections, we will introduce our implementations for different boundary conditions.

2.2.1 Mass Flow Rate Boundary Condition

In some cases, such as rooms with a mechanical ventilation system, the inlet mass flow rate \dot{m}_{inlet} at the inlet can be specified. As shown in Figure 2, as one inlet is facing towards an outlet, a strong momentum effect takes place at the outlet in *Zone 1*. Thus *Zone 1* is a candidate for simulation using FFD to express the unevenly distributed mass flows at

the outlets (Wang and Chen 2007). *Zone 2* and *Zone 3* are then simulated by the multizone models. Regarding the exchange data, the flow rate ($\dot{m}_{in_1}, \dot{m}_{in_2}, \dots, \dot{m}_{in_i}$) and temperature ($\varphi_{in_1}, \varphi_{in_2}, \dots, \varphi_{in_i}$) at inlets are fed to FFD and FFD gives the flow rate ($\dot{m}_{out_1}, \dot{m}_{out_2}, \dots, \dot{m}_{out_j}$) and temperature ($\varphi_{out_1}, \varphi_{out_2}, \dots, \varphi_{out_j}$) at outlets back to the multizone model, as follows:

$$\mathbf{x}_1 = \{\dot{m}_{in_1}, \dot{m}_{in_2}, \dots, \dot{m}_{in_i}, \varphi_{in_1}, \varphi_{in_2}, \dots, \varphi_{in_i}\} \quad (8)$$

$$\mathbf{x}_2 = \{\dot{m}_{out_1}, \dot{m}_{out_2}, \dots, \dot{m}_{out_j}, \varphi_{out_1}, \varphi_{out_2}, \dots, \varphi_{out_j}\} \quad (9)$$

where i and j are the numbers of the inlet and outlet in FFD, respectively; \dot{m} is the mass flow rate; φ is the scalar variable such as temperature and trace substance concentration.

Receiving \mathbf{x}_1 , at the inlet, FFD calculates the velocity at inlets based on the mass flow rates ($\varphi_{in_1}, \varphi_{in_2}, \dots, \varphi_{in_i}$) and applies the velocity and temperature as Dirichlet boundary conditions for inlets. Finally, for the outlet, FFD applies Neumann boundary conditions. None-slip wall is used in FFD. Once completing the simulation for one data synchronization time step, FFD feeds the mass flow rate at the outlets

($\dot{m}_{out_1}, \dot{m}_{out_2}, \dots, \dot{m}_{out_j}$) to calculate the pressure (P_2, P_3) at the other zones and the mass flow rate ($\dot{m}_{20}, \dot{m}_{30}$) at the other openings based on Equation (6).

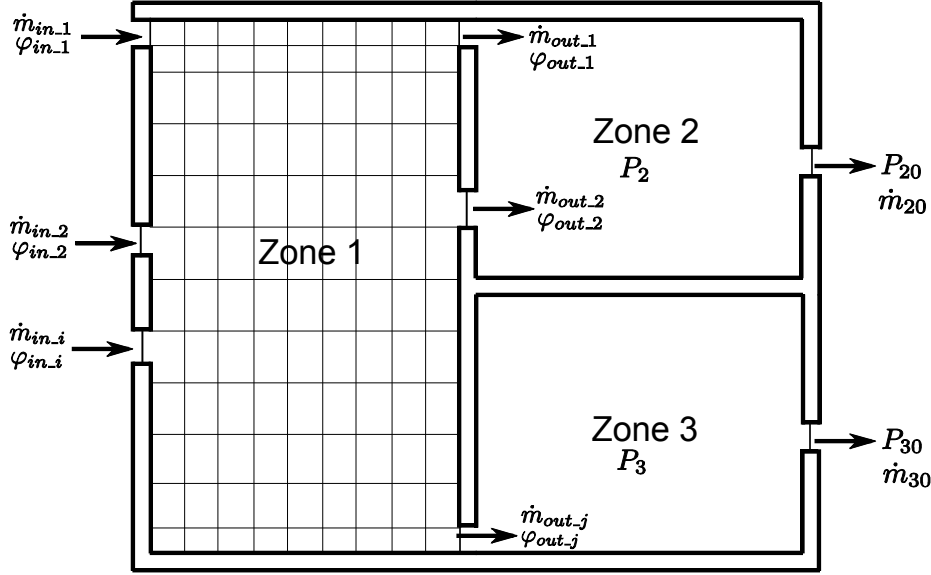


Figure 2 Sketch of the case where a velocity boundary condition is applied

2.2.2 Total Pressure Boundary Condition

On other occasions such as wind-driven natural ventilation, the mass flow rate at the inlet of the CFD zone cannot be directly obtained. Instead, the total pressure can be derived from measuring at the upstream point. In contrast, as shown in Figure 3, despite that the mass flow rate at the inlet of *Zone 1* may be known, the mass flow rate \dot{m}_1 at inlet of *Zone 3*, which is simulated using FFD, is unknown prior to the calculation of multizone model. *Zone 1*, *Zone 2* and *Zone i* are simulated by the multizone model. As show in Equations (10) and (11), the multizone model gives the pressures (P_1, P_2, \dots, P_i) and other scalar variables ($\varphi_{M_1}, \varphi_{M_2}, \dots, \varphi_{M_i}$) at all openings to FFD. FFD will use the sign of the mass flow rates calculated by Modelica to determine if the openings are inlets or outlets. Then after that, FFD will only use the temperatures at the inlet for calculation, as for outlets it applies a Neumann (zero-gradient) boundary condition for temperature. Upon completing the calculation for one data synchronization time step, FFD transfers the mass flow rates

$(\dot{m}_1, \dot{m}_2, \dots, \dot{m}_i)$ and scalar variables $(\varphi_{F_1}, \varphi_{F_2}, \dots, \varphi_{F_i})$ at all elements of the multizone model. In the equations below, i represents the number of openings in the CFD simulation.

$$\mathbf{x}_1 = \{P_1, P_2, \dots, P_i, \varphi_{M_1}, \varphi_{M_2}, \dots, \varphi_{M_i}\} \quad (10)$$

$$\mathbf{x}_2 = \{\dot{m}_1, \dot{m}_2, \dots, \dot{m}_i, \varphi_{F_1}, \varphi_{F_2}, \dots, \varphi_{F_i}\} \quad (11)$$

Wang and Chen (2005) showed that by exchanging total pressure and mass flow rate between multizone model and CFD, it is feasible to achieve converged results between coupled models.

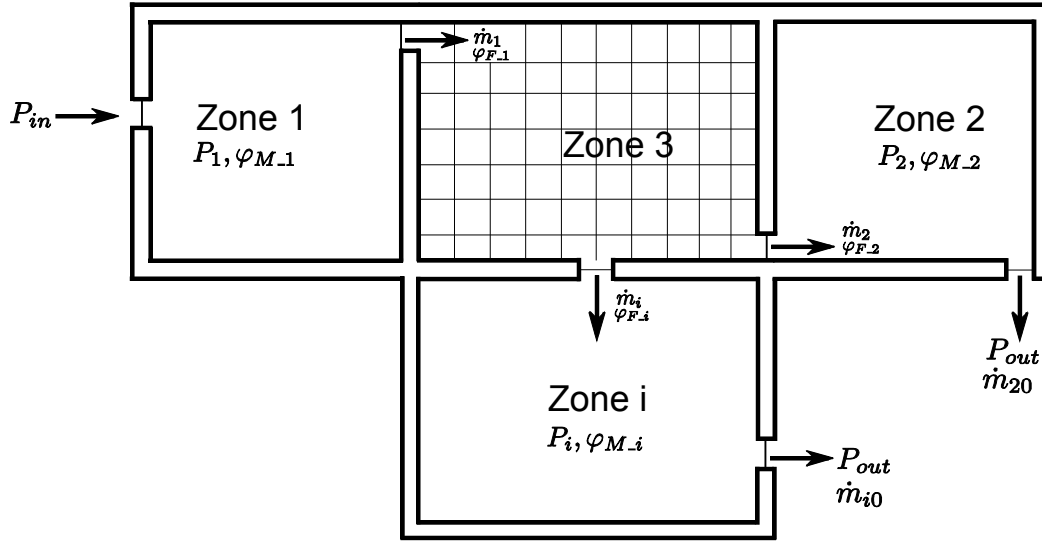


Figure 3 Sketch of the case where a total pressure boundary condition is applied

After receiving the \mathbf{x}_1 from the multizone model, FFD will calculate the mass flow rate and values of scalar variables at all openings. In lieu of velocity as a boundary condition for inlets, static pressures are used together with the temperatures at inlets for FFD to determine the mass flow rates $(\dot{m}_1, \dot{m}_2, \dots, \dot{m}_i)$ and temperature $(\varphi_{F_1}, \varphi_{F_2}, \dots, \varphi_{F_i})$ at all openings. The details of how FFD applies pressure boundary conditions to openings will be introduced in section 3.2. Finally, FFD sends that information as \mathbf{x}_2 back to the

multizone models. The multizone models will then determine the total pressure (P_1, P_2, P_i) and temperature ($\varphi_{M_1}, \varphi_{M_2}, \dots, \varphi_{M_i}$) at other zones and the mass flow rates ($\dot{m}_{20}, \dot{m}_{i0}$) at other openings in the systems.

3 Implementation of the coupled FFD and Multizone Models

This chapter introduces the implementation of coupling strategies in section 2.2. Previously, Zuo et al. (2016) presented a coupling framework between Modelica and CFD (using the FFD program as an example) to study the heat transfer through building envelopes, HVAC operation and control, and airflows in buildings. FFD was compiled as a dynamic linker and called by Modelica once the simulation was being executed. The coupling framework named as *Rooms.CFD* was later publicly released along with the Modelica *Buildings* library. The implementations in this paper are dependent on that work.

3.1 Implementation with Mass Flow Rate Boundary Condition for FFD

Figure 4 shows the schematic of the first coupling strategy which applies mass flow rate as a boundary condition to FFD. The icon named *CFD Zone* is an instance of a type of *Rooms.CFD*, which interfaces between Modelica and FFD. On one hand, the model *CFD Zone* calculates the mass flow rates at all fluid ports, which are *Port 1* (the fluid port connected to the inlet) and *Ambient* (fake boundaries whose number is equal to that of the outlet in *CFD Zone*), in this case, using a mixing volume assumption. Note that the outlet *Ambient* is connected to *CFD Zone* through a *Resistance* (a model regressing the pressure drop and the mass flow rate), as this is to guarantee that the equation sets governing the mixing volume are fully closed when the number of outlets exceeds two. Receiving the mass flow rates, FFD will first assign “inlet” and “outlet” tags to openings based on the

sign of mass flow rate. Afterward, it can assign the corresponding boundary conditions. Similarly, the *Heat port* is connected to the *CFD Zone* to provide the thermal boundary conditions of the walls to FFD.

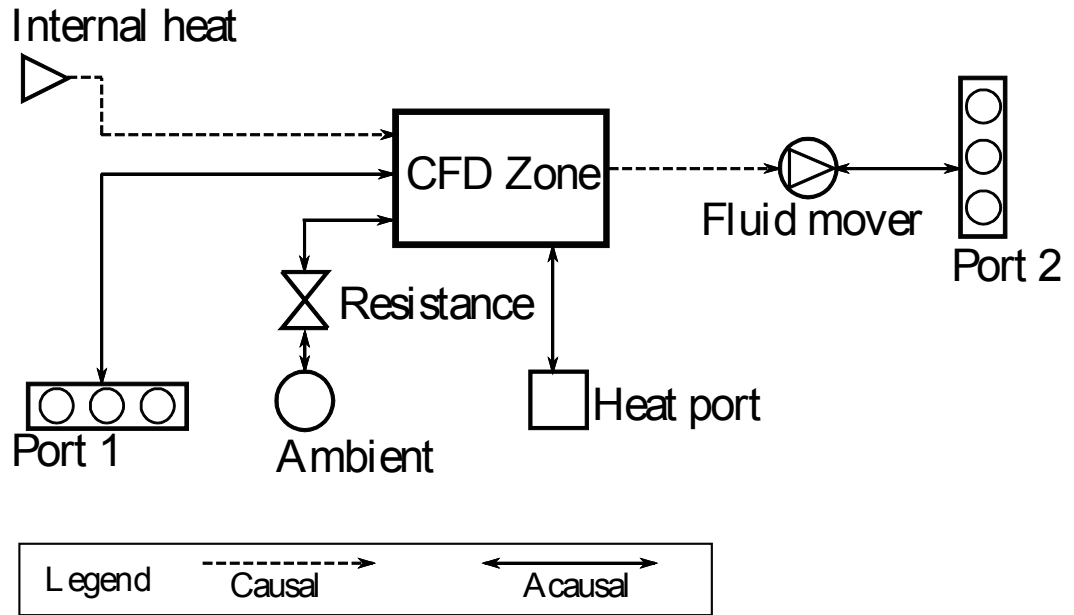


Figure 4 Schematic of coupling strategy in Modelica when velocity boundary condition is applied to FFD

On the other hand, FFD sends the exchange data quantities back to Modelica through the *CFD Zone*. The mass flow rates and temperature at the outlet fed to a prescribed mass flow rate *Fluid mover*. The *Fluid mover* works as an ideal flow source that can provide any user-provided values of flow rate, temperature, composition and trace substance. The *Fluid mover* is further connected to *Port 2* (fluid ports connected to the outlets, namely, the inlets of the multizone models), which is used as an interface to connect the outside fluid port.

Figure 5 illustrates the Modelica implementation of the first coupling strategy. Note that the mass flow rates at the outlet are connected to a prescribed mass flow rate *Fluid*

mover through a first order delay, which is used to avoid model failure. Additionally, the sensor information is sent out through an output icon to facilitate the modeling of the control. The FFD implementation is the same as that in the coupling platform presented in the literature (Zuo et al. 2016).

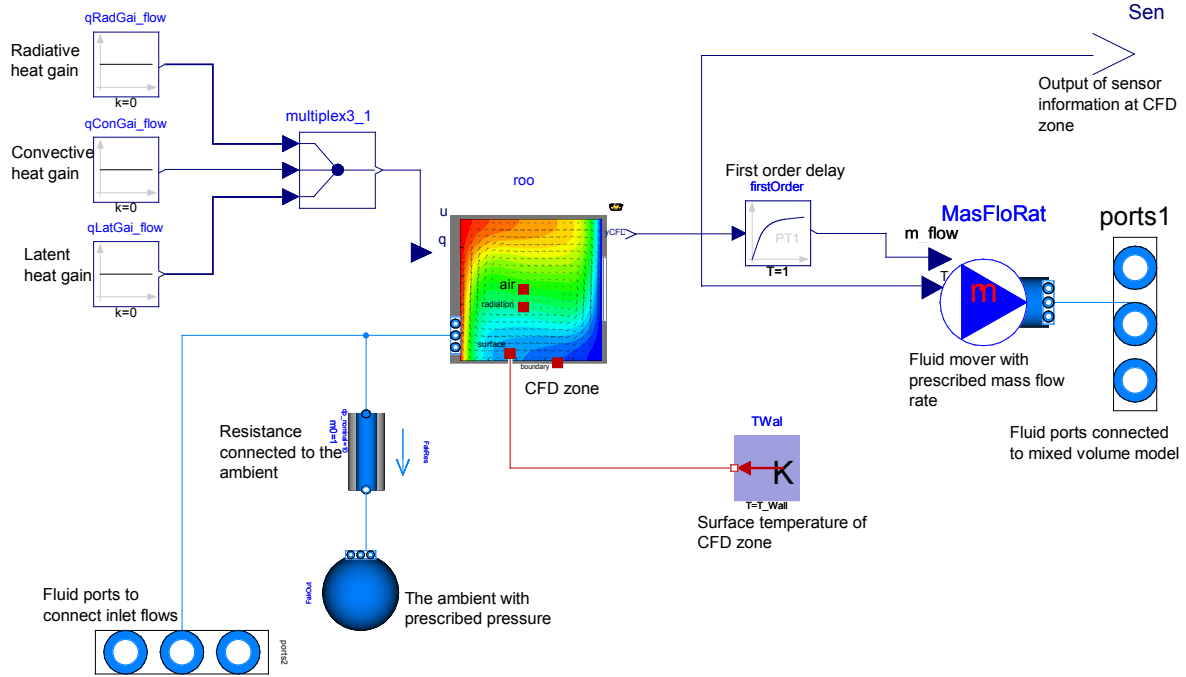


Figure 5 Implementation of coupling strategy in Modelica when a velocity boundary condition is applied to FFD

3.2 Implementation with Total Pressure Boundary Condition for FFD

Compared to the previous implementations, the total pressure at the fluid ports is sent to FFD from Modelica and the mass flow rate at all ports are sent from FFD to Modelica. Though largely based on the first implementation, as is illustrated in Figure 4, the schematic of the implementation shown in Figure 6 differs from the previous implementation in following aspects: first, an additional mixing volume called *Volume 1* is added to receive the pressure (P) and temperature (T) information at the “upstream” zone while *Volume 2*, which previously was *Ambient*, is now used to collect the pressure (P)

information at the “downstream” zone. Second, as FFD gives the information of flow rates at all openings back to *CFD Zone*, another port called *Port 2* is created to be connected to the upstream openings (inlet). Similarly, *Port 2* is connected to a *Fluid mover*, which receives information of flow rate and temperature information from *CFD Zone*.

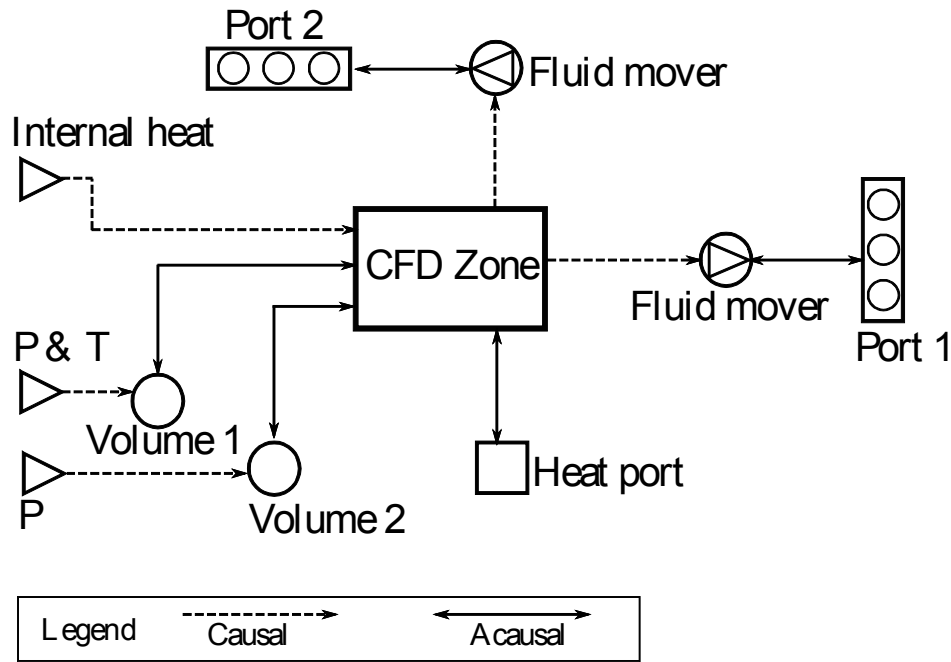


Figure 6 Schematic of coupling strategy in Modelica when total pressure boundary condition is applied to FFD.

Figure 7 shows the Modelica implementation of coupling strategy with total pressure being applied to FFD. Note that to avoid redundancy, vectors are being applied to many models such as mixing volumes, fluid movers, first order delays, etc. Figure 8 shows the implementation of total pressure boundary conditions in the FFD program when it is coupled with the multizone model implemented in Modelica. Receiving the pressure at inlets and outlets from Modelica (P_{in} , P_{out}), FFD applies the total pressure P_{out} for outlets directly. For inlets, FFD assumes an initial velocity at the inlet at the beginning of the

simulation, and calculates the static pressure P_{static} as a boundary condition for the inlet based on the Bernoulli's principle. Afterward, the FFD algorithm is executed by sequentially solving the advection, diffusion, and projection equation. Consequently, the velocity at the inlet will be updated after each iteration. If the data synchronization point is reached, FFD writes the information to Modelica and receives updated total pressures from Modelica.

Figure 7 Implementation of coupling strategy in Modelica when total pressure boundary condition is applied to FFD.

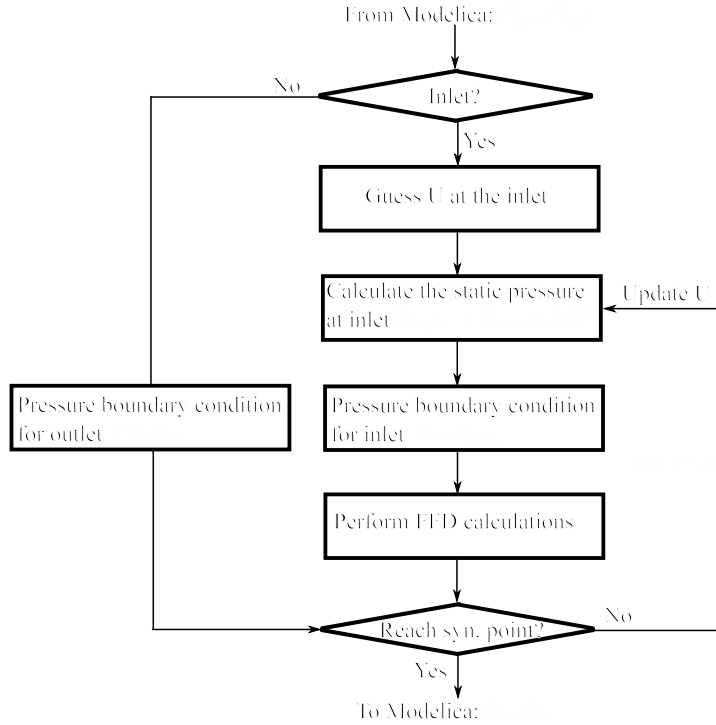


Figure 8 Total pressure implementation in FFD

4 Performance Assessment and Validation

The implementations in Modelica of coupling FFD and multizone models were further validated using two experiments by Wang and Chen (2007). One case is an isothermal flow involving a non-uniform momentum distribution and the other one is a non-isothermal flow involving a non-uniform temperature distribution.

4.1 Validation 1: Isothermal Flow with Non-Uniform Momentum Distribution

The isothermal flow case is used to validate the first coupling implementation in section 3.1. Figure 9 shows the sketch of the test room involving the non-uniform momentum distribution since the inlet is directly facing *Opening 1* at *Zone 1*, which is simulated by FFD. The size of *Zone 1* is 4.93 m × 1.83 m × 2.44 m. The inlet is 0.3 m × 0.2 m, and the sizes of *Opening 1* and *Opening 2* are the same (0.4 m × 0.2 m). The flow rate at

the inlet varies from 73, 113, 223, 296, and 456 CFM (or 0.033, 0.053, 0.105, 0.14, and 0.215 m³/s) at different scenarios.

In the FFD simulation, a mesh size of $34 \times 12 \times 18$ was used. The time step size was 0.1s for when the flow rates were 0.033 and 0.053 m³/s and 0.05s for others. To simulate the turbulence effect introduced by the high-velocity jet, we employed a zero equation model proposed by Chen and Xu (1998). However, we adjusted the α coefficient to 0.00874 in Equation (12), in which ρ , V , l are density, local mean velocity, and a length scale, respectively.

$$\mu_t = \alpha \rho V l. \quad (12)$$

This is because compared to the CFD, the splitting of Navier-Stokes equations in FFD introduces numerical viscosity (Zuo et al. 2012). Finally, we turned off the energy equation to simulate the case as a forced convection. For other detailed information about the case setup, one can refer to the literature (Wang and Chen 2007).

The Modelica representation of the case is shown in Figure 10. *Zone 1* was simulated by FFD while other zones were studied by multizone model, simply represented by using a *MixingVolume* model from the *Buildings* library. The model named *Zone_1* in Figure 10 is the instance of the class introduced in section 2.3.1. The inlet airflow was provided by a prescribed mass flow rate fluid mover model that was connected to the fluid ports of *Zone_1*. The opening on the surfaces of the zones was modeled by the *Orifice*, which was implemented based on the Equation (6). The data synchronization time step was set as 5 s.

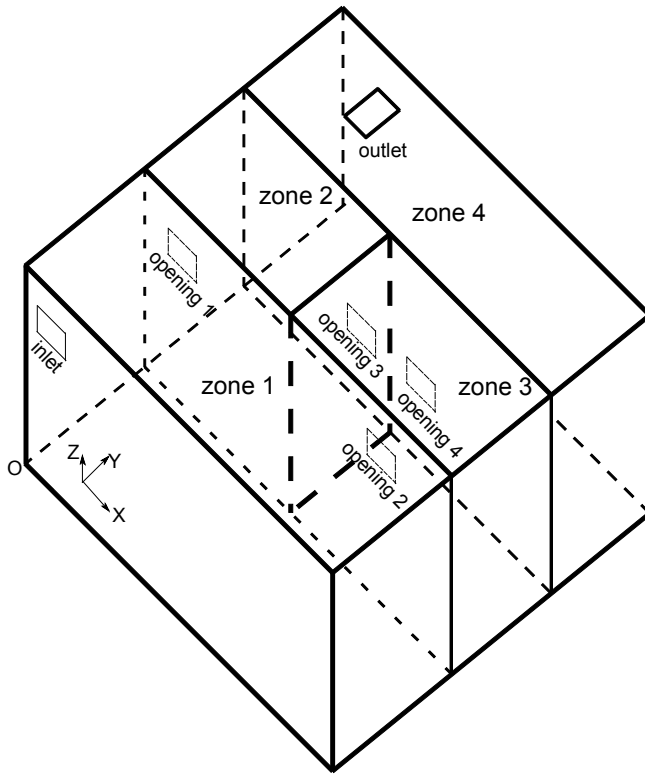


Figure 9 Sketch of the isothermal case for validation

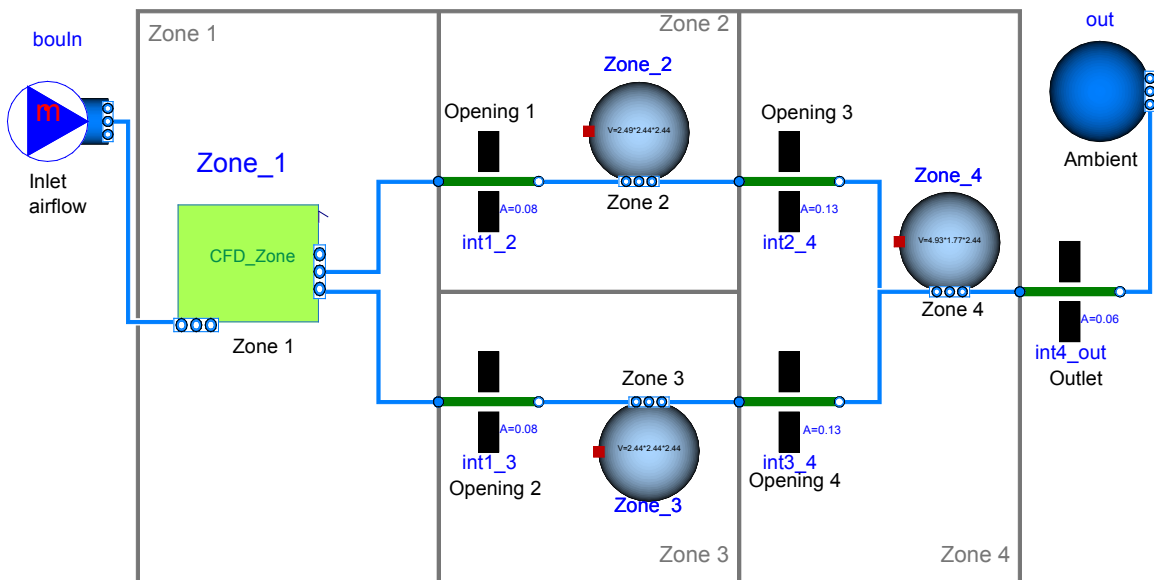


Figure 10 Modelica model of the isothermal case for validation

Then the model was compiled and ran in Dymola 2016 with Microsoft Visual Studio 2013 as the compiler. The a Radau 5th order scheme was used as the solver and the tolerance was set as 10^{-6} . The simulation time was 100 s. Figure 11 shows the flow rate ratio of *Opening 1* and *Opening 2* in *Zone 1* under different inlet flow rates. The simulated results show a good agreement with the experiment when the inlet mass flow rate is generally larger. This is due to the fact that the numerical viscosity in FFD is associated with the grid resolution and it becomes relatively smaller compared to the turbulent viscosity when the velocity of inlet jet is high. Interestingly, the results from our coupling model are better than those from Wang and Chen (2007), which coupled the CFD program with the CONTAM. One of the possible reasons is that we tuned the coefficients of the zero equation turbulence model for FFD using one of the five cases.

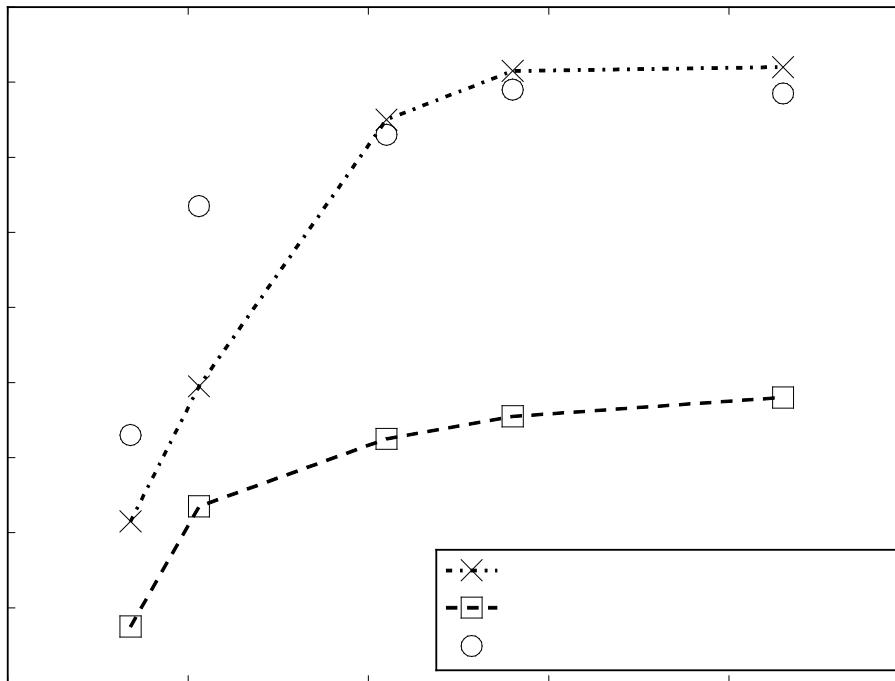


Figure 11 Comparison of mass flow ratios predicted by coupling FFD and multizone, simulation of Wang and Chen (2007), and experimental data for case 4.1

Figure 12 shows the Modelica results of the mass flow rate at the openings and the pressure in the zones under a flow rate of $0.033 \text{ m}^3/\text{s}$. The flow rate at *Opening 1* and *Opening 2* were 0.020 and 0.013 kg/s at the time of 30 s , when the flow was estimated to be fully developed. Due to the mass conservation law, *Opening 1* had same airflow rate as *Opening 3* and so did *Opening 2* as *Opening 4*. The pressure at *Zone 2* is slightly higher than *Zone 3* due to the higher air flow rate. Note that in the first 5 seconds of the simulation the mass flow rate and pressure are zero as zero initial values are applied to the air flow rates of *Opening 1* and *Opening 2*.

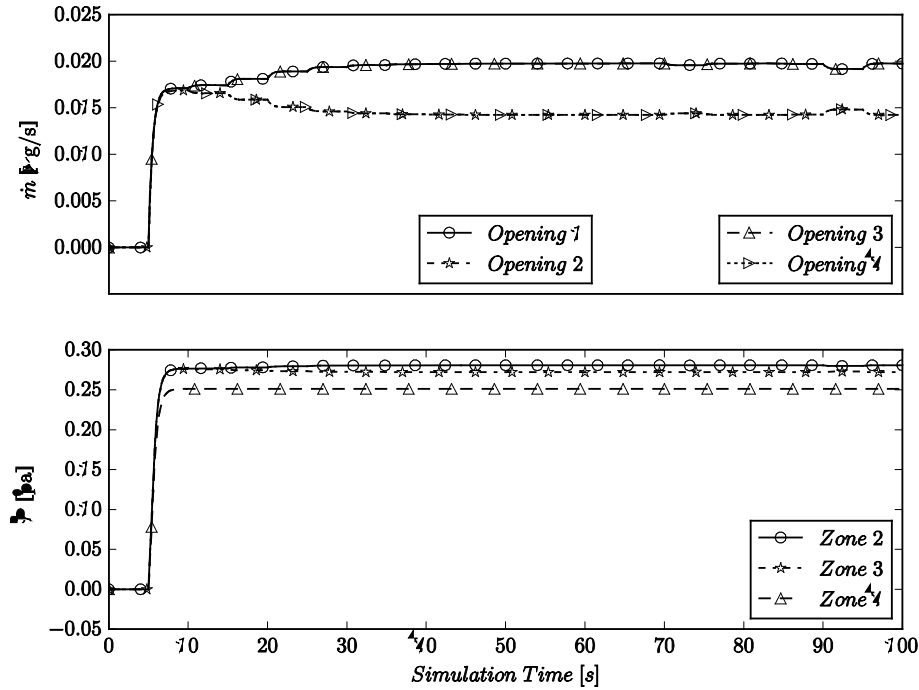


Figure 12 Mass flow rates and room pressures calculated by Modelica models in case 4.1

4.2 Validation 2: Non-Isothermal with Non-Uniform Temperature Distribution

The non-isothermal case is used to validate the second coupling implementation in section 3.2. Figure 13 shows the sketch of the test room that is modified based on the previous case. In the new case, *Zone 2* and *Zone 3* contain two identical blocks symmetrically located near the interior corner. The block in *Zone 2* is heated while the block in *Zone 3* is not. The dimensions of the blocks are $0.4 \text{ m} \times 0.25 \text{ m} \times 0.5 \text{ m}$. An additional inlet (*Inlet 2*) was also added at *Zone 1* and the size is $0.3 \text{ m} \times 0.2 \text{ m}$ which is identical to the *Inlet 1*. Finally, *Zone 2* is $2.49 \text{ m} \times 2.44 \text{ m} \times 2.44 \text{ m}$. Since the block surface temperature at *Zone 2* is higher than the air a non-uniform temperature distribution was formed, thus *Zone 2* was simulated by FFD. Three scenarios were tested, in which the flow rate and temperature at the inlet of *Zone 1* and the block surface temperature in *Zone 2* were varied. The variations are shown in Table 1.

Table 1 Boundary conditions for FFD for the non-isothermal case 4.2

Scenario #	1	2	3
Flow Rate at <i>Inlet 1</i> (m^3/s)	0.0477	0.051	0.0514
Temperature at <i>Inlet 1</i> ($^{\circ}\text{C}$)	18.5	18.9	18.5
Flow Rate at <i>Inlet 2</i> (m^3/s)	0.0543	0.0467	0.0533
Temperature at <i>Inlet 2</i> ($^{\circ}\text{C}$)	18.5	18.7	18.3
Block Surface Temperature	30	35	46

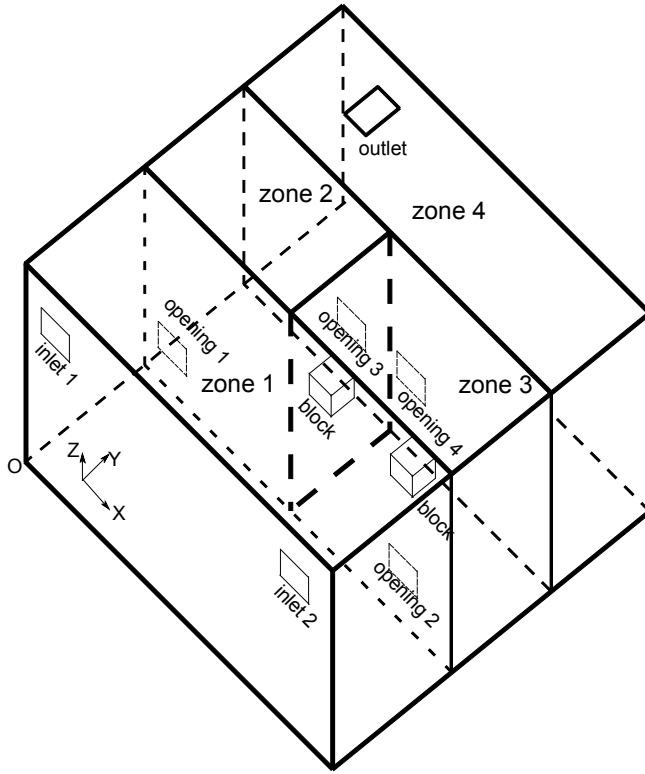


Figure 13 Sketch of the non-isothermal case for validation

In the FFD simulation, we used a mesh of $24 \times 24 \times 24$. The time step size was 0.05 s. Again, the zero-equation model with the same coefficients as the previous case was employed. We used the Boussinesq assumption to account for the buoyant force caused by the temperature difference.

The Modelica implementation of the non-isothermal validation case is shown in Figure 14. The model named *Zone_2* is the instance of the model presented in Figure 7. *Zone 1*, *Zone 3*, and *Zone 4* were simulated by the *MixingVolume*. A pressure and a static temperature sensor were put at the upstream of *Zone 2* and also a pressure sensor was fixed at the downstream. The information from those sensors was provided to FFD as the boundary conditions at the openings. For other parts of the model, they were like the previous case.

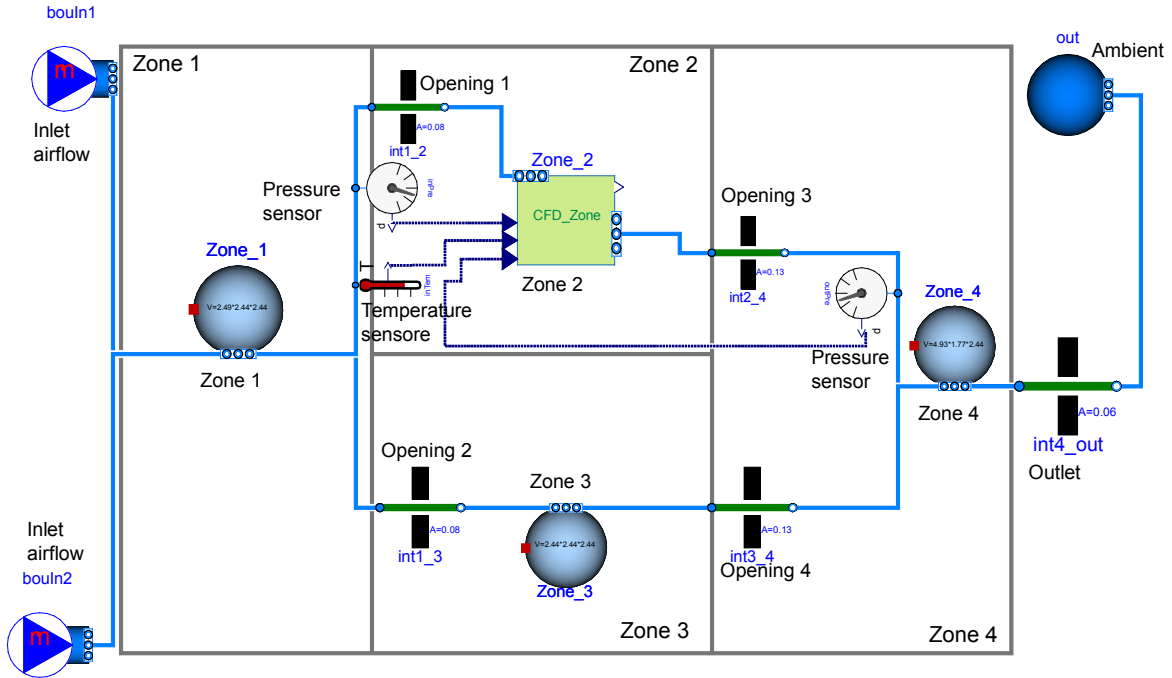


Figure 14 Modelica model of the non-isothermal case for validation case 4.2

The solver and compiler settings are identical to the previous case. The simulation time is 1000 s. Figure 15 shows the flow rate ratio at *Opening 3* and *Opening 4* in three different scenarios. Thanks to a larger pressure near the outlet induced by the stack effect, there was more air flowing out of the outlet in *Zone 2* than *Zone 3*. As the block surface temperature increased from 30 to 46 °C, the magnitude of the stack effect increased, and consequently the flow rate ratio of *Opening 1* compared to *Opening 2* increased accordingly from 1.23 to 1.46. The simulated results were in good accordance with the experimental data, except for the first scenario. Our results agreed with those from Wang and Chen (2007), and they attributed the large discrepancy in the first scenario to a measurement error.

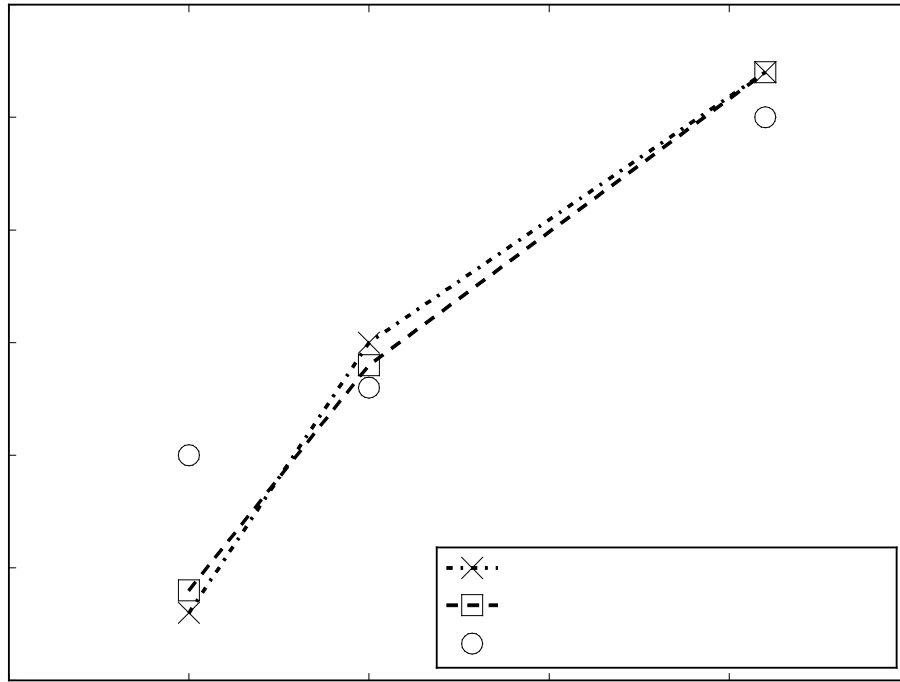


Figure 15 Comparison of mass flow ratios predicted by coupling FFD and multizone, simulation of Wang and Chen (2007), and experimental data for case 4.2

Physically, for the whole space, the total pressure at zones and the flow rates at openings were fully coupled. As the initial values were assigned to the flow rates at openings, the pressure at all zones was determined. With the updated pressure information, the flow rate can be obtained. Usually, several iterations were needed to find the correct solution of pressure and flow rates as the calculation tended to be stabilized. Figure 15 shows the Modelica results of the flow rate at openings and pressure at zones for the scenario #1. The initial value of zero was given to *Opening 1* and *Opening 3*, and initial flow rates at *Opening 2* and *Opening 4* were large (0.104 kg/s). They were identical due to the mass conservation. This further formed a large pressure difference of 4.0 Pa between *Zone 1* and *Zone 4*. With a large pressure difference fed to FFD, the mass flow rates at

Opening 1 and *Opening 3* were determined to be 0.092 kg/s. After FFD sent these mass flow rates to the multizone model, the flow rate at *Opening 2* and *Opening 4* decreased from the initial value of 0.104 to 0.012 kg/s and the pressure difference between *Zone 1* and *Zone 3* consequently decreased from 4.0 to 3.6 Pa. With several iterations, the magnitude of the fluctuations of mass flow rate and pressure decreased gradually and the simulation approached to the converged solution after about 300s. Eventually, the mass flow rates at *Opening 1* and *Opening 2* were 0.05633 and 0.04567 kg/s, which led to a flow rate ratio of 1.23.

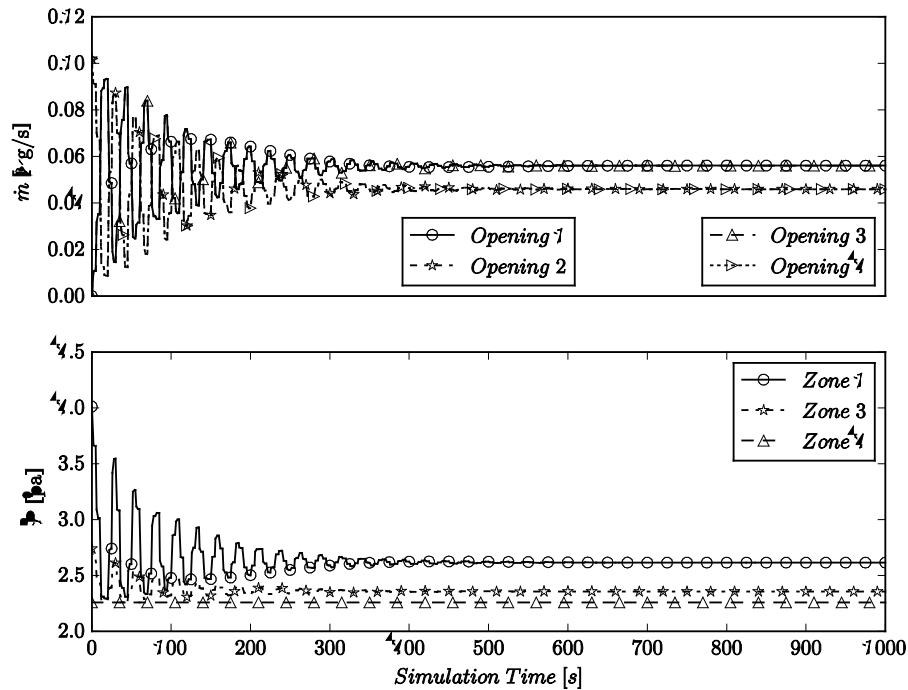


Figure 16 Mass flow rates and room pressures calculated by Modelica models in case 4.2

5 Case Studies

In this section, we performed three case studies to show that the coupled FFD-multizone model can be used to study the dynamic response of an HVAC system. We

started with adding a VAV terminal box to previously validated cases. Afterward, we further increased the complexity of the cases by adding a VAV system to the flow.

5.1 Flow with Non-Uniform Momentum Coupled to A VAV Terminal Box

Based on the airflow network model in Figure 10 in section 4.1, this case study added a VAV terminal box to substitute the prescribed fluid movers connected to *Zone 1*, as shown in Figure 17. The control objective of the VAV terminal box is to sustain 25 °C temperature for occupant zone of *Zone 1*, which is the lower half part ($Z \leq 1.22$ m). To increase the efficiency of temperature control, we increased the length of the inlet (in the X direction) by 0.53 m. The surface temperatures for floor and other walls in *Zone 1* are 25 °C and 27 °C, respectively. The initial temperatures of all the zones is 30 °C.

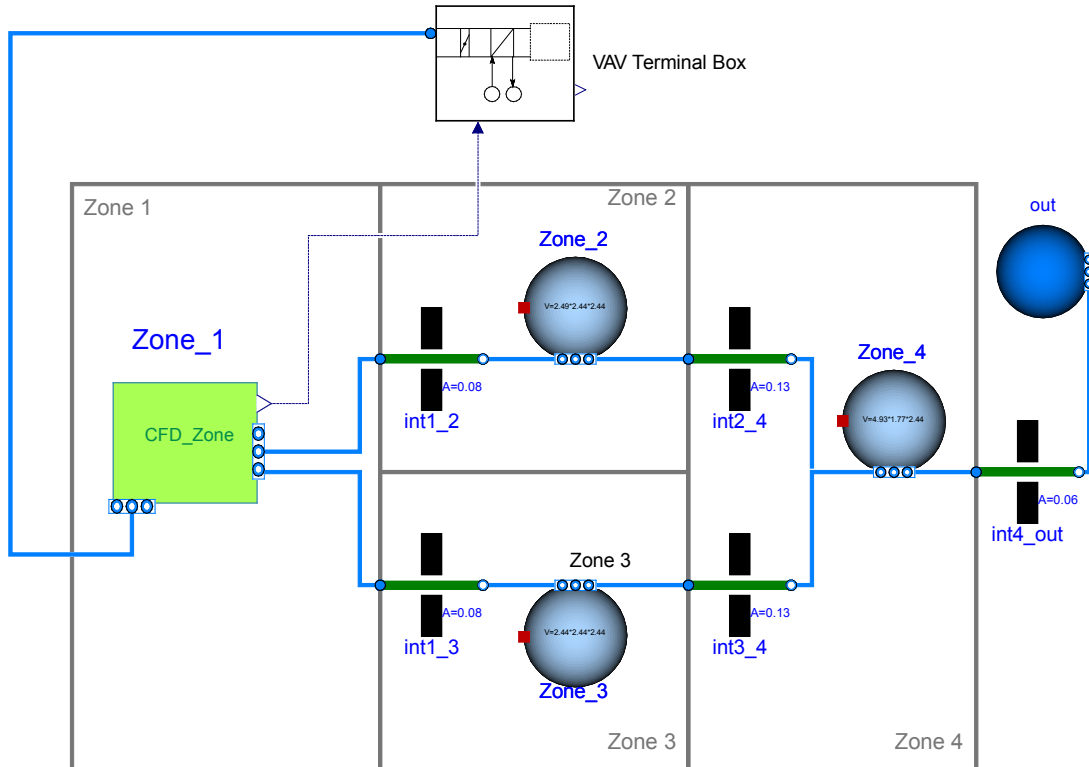


Figure 17 Top level diagram of Modelica models for case 5.1 VAV terminal box for space with non-uniform momentum

Figure 18 illustrates the detailed Modelica model of VAV terminal box based on *Examples.VAVReheat.ThermalZones.VAVBranch* in the Modelica Buildings library. The model consists of a cold air source, a water-air heat exchanger with a valve in the water loop, an adjustable valve in the air loop, a controller, and multiple sensors. Since we isolated the room from a VAV system which serves multiple rooms, we assumed that the pressure difference at terminal box and space outlet was constant. Thus, we set the relative pressure (to the ambient pressure of 101 kPa) and pressure and temperature of the cold air source as 20 Pa and 16 °C, respectively. The supply water temperature is set to be 50 °C. The pressure difference at the water source and water sink is 12,000 Pa. Based on the actual room temperature and opening of the valve in the air loop, the controller can adjust the opening ratio of the valve in both air and water loops. If the minimal air flow rate is still too large for the cooling needs, the heat exchanger can heat up the air once the valve in the water loop is turned on.

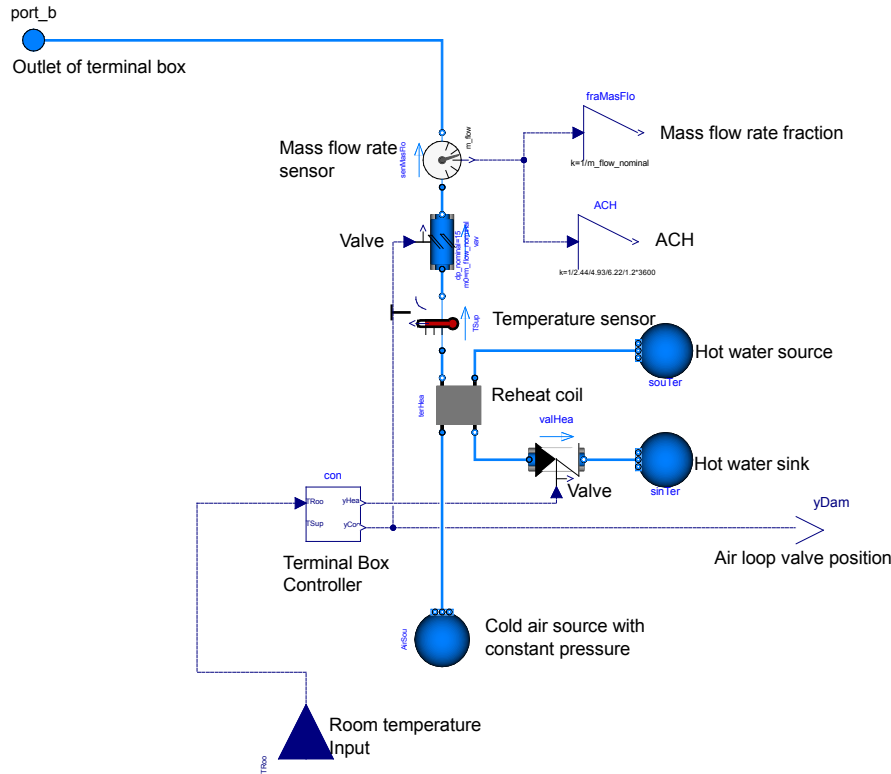


Figure 18 VAV terminal box

As shown in Figure 19, we implemented a pressure-dependent control logic (Liu et al. 2012) as an example based on *Examples.VAVReheat.Controls.RoomVAV*. The occupant zone temperature signal is first sent to adjust the valve position in the air loop, which is at the lower part of the figure. A PI controller was employed to determine the signal. If the valve opening decreases to 30% (deemed as the lower limit) and the actual room temperature does not reach the set point, the reheat coil will turn on by feeding the opening position signal to the valve in the water loop. The control of the reheat coil is shown in the upper part of the figure. Similarly, another PI controller was used to determine the signal. To avoid the short cycling of the reheat coil, we added hysteresis to the controller which has a lower bound of 0.3 and a higher bound of 0.4. With hysteresis, when the reheat was

turned on and the opening signal to the valve in the air loop was between 0.3 and 0.4, the reheat of air continued.

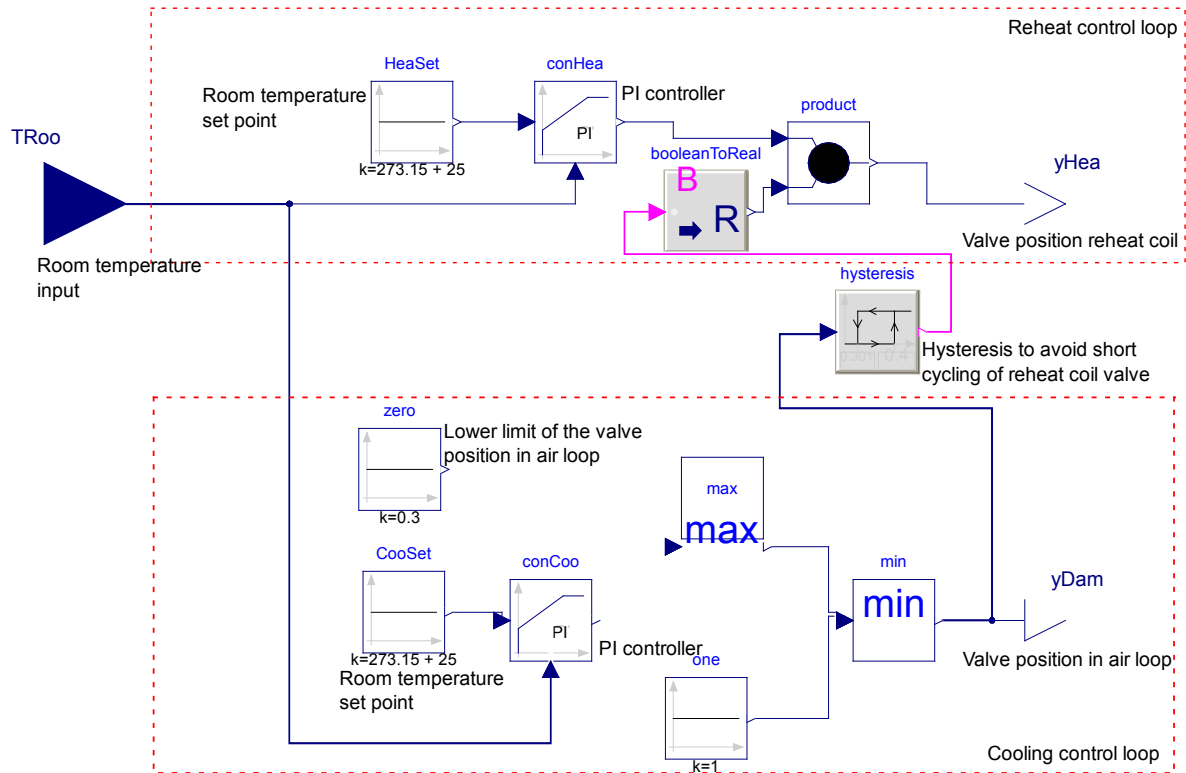


Figure 19 Controller in VAV terminal box

The case was simulated for 900 seconds using identical settings of solver and tolerance as previous case. From Figure 20a-d, the dynamic response of the VAV terminal box and indoor environment are shown. In the beginning, as shown in Figure 20a, the room temperature is initially higher than the set point (25 °C), the opening ratio of the valve in the cold air loop decreases from 1.0 to 0.3 as shown in Figure 20b. The mass flow rate of the supply air as shown in Figure 20c then drops from 0.120 kg/s to 0.044 kg/s. Since the reheat coil does not turn on, the supply air temperature remains constant at 16 °C, as shown in Figure 20d.

At around 60 seconds, when the opening ratio of the valve in the cold air loop reached 30%, and the room temperature was lower than the set point (Figure 20 a), the reheat coil is turned on. Then, the room temperature increases. However, it is still lower than the set point over the period from 60-160 s. Here, the opening ratio of the valve in cold air loop remains at the minimum of 30% and the opening of the valve in the reheat coil changes accordingly with the actual room temperature, as shown in Figure 20b. Consequently, one can see in Figure 20d that the supply air temperature first increases to a maximum of 25.4 °C and then gradually drops to 23.0 °C, along with the change in the valve opening of the reheat coil.

From 160 to 225 seconds, the room temperature is higher than the set point and their difference is decreasing (Figure 20a). However, due to the hysteresis embedded in the controller and the opening of the valve in air loop being less than 0.4, the reheat coil remained on with a small opening (Figure 20b). Thus, the supply air temperature was higher than 16 °C and generally decreased with the valve opening becoming smaller (Figure 20d).

After approximately 225 seconds, the room temperature approached the set point (Figure 20a). At end of the simulation, the difference between room temperature and the set point is marginal. Since the room temperature is higher than set point and the opening of the valve in air loop is larger than 0.4, the reheat coil turns off (Figure 20b) and supply air temperature remains at 16 °C (Figure 20d).

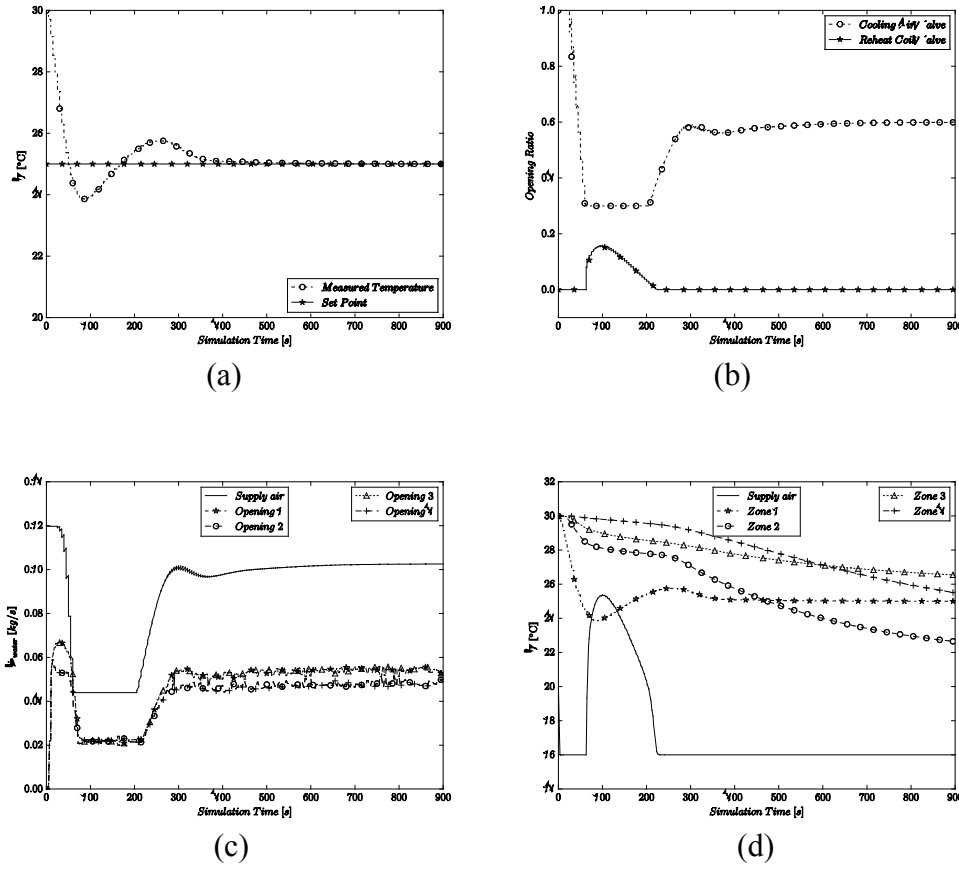


Figure 20 (a) Zone 1 temperature control; (b) Control outputs from VAV terminal box; (c) Mass flow rates at different openings; (d) Zone temperature in the space

Note that we presented the mass flow rate of the supply air at different openings in the space in Figure 20c. We can clearly identify the mass flow rate difference at *Opening 1* and *Opening 2*, which would be ignored if a multizone model were used. Due to the mass conservation law, the mass flow rate at *Opening 1* and *Opening 3* are equal, and the same rule applies to *Opening 2* and *Opening 4*.

5.2 Flow with Non-Uniform Temperature Coupled to A VAV Terminal Box

Based on the model (Figure 14) presented in section 4.2, this case study adds a VAV terminal box to substitute the prescribed fluid movers connected to *Zone 1*, as shown

in Figure 21. The VAV terminal box was set to control the temperature of *Zone 2* as 25 °C. The surface temperature for the floor and other walls in *Zone 2* are 25 °C and 27 °C, respectively. The initial temperature of *Zone 1* and the other spaces are 25 °C and 30 °C, respectively. The VAV terminal box model is identical as the one in section 4.3.

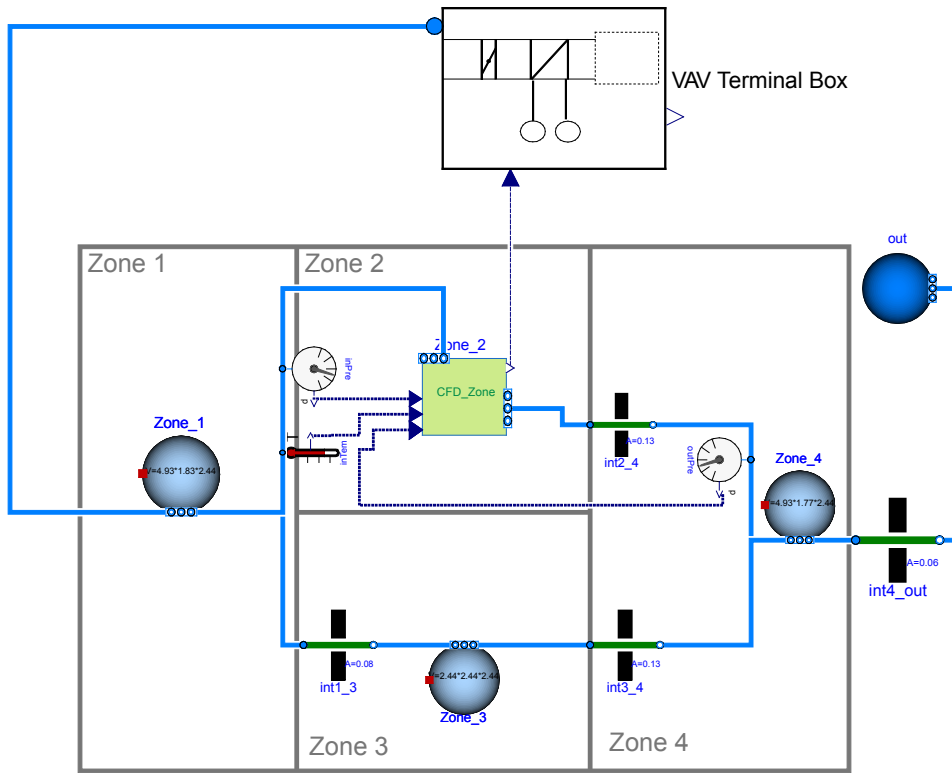


Figure 21 VAV terminal box for space with non-uniform temperature distribution

The case was simulated for 1800 seconds using identical settings for the solver and tolerance as in the previous case. Figure 22a-d show the results of the temperature control for *Zone 2*, control outputs of the VAV terminal box, the mass flow rate at different openings, and temperature in the zones. Since *Zone 2* is connected to *Zone 1* via *Opening 1*, the temperature at *Zone 2* decreases during the first 1000 seconds, in conjunction with the temperature at *Zone 1*, as shown in Figure 22d. As *Zone 2* is cooled by the cold air from *Zone 1*, the opening ratio of the valve in the air loop in the VAV terminal box is gradually

turned down from 1.0 to 0.3. Consequently, the mass flow rate of the supply air is reduced from 0.110 kg/s to 0.044 kg/s, which consequently decreases the flow rate of cold air into *Zone 2* and *Zone 3*. At around 1000 s, thanks to that the actual temperature of *Zone 2* being lower than the set point of 25 °C and the opening of the valve in the air loop reaching the minimal value, the VAV terminal box modulates to reheat the supply air, as shown in Figure 22b. As a result, the supply air temperature and temperature in *Zone 1* increases. Afterward, the opening ratio of the valve in the air loop increases and the reheat is terminated as it reaches to 0.4. Eventually, *Zone 2* is air-conditioned to the desired temperature of 25 °C with high control precision, as shown in Figure 22a.

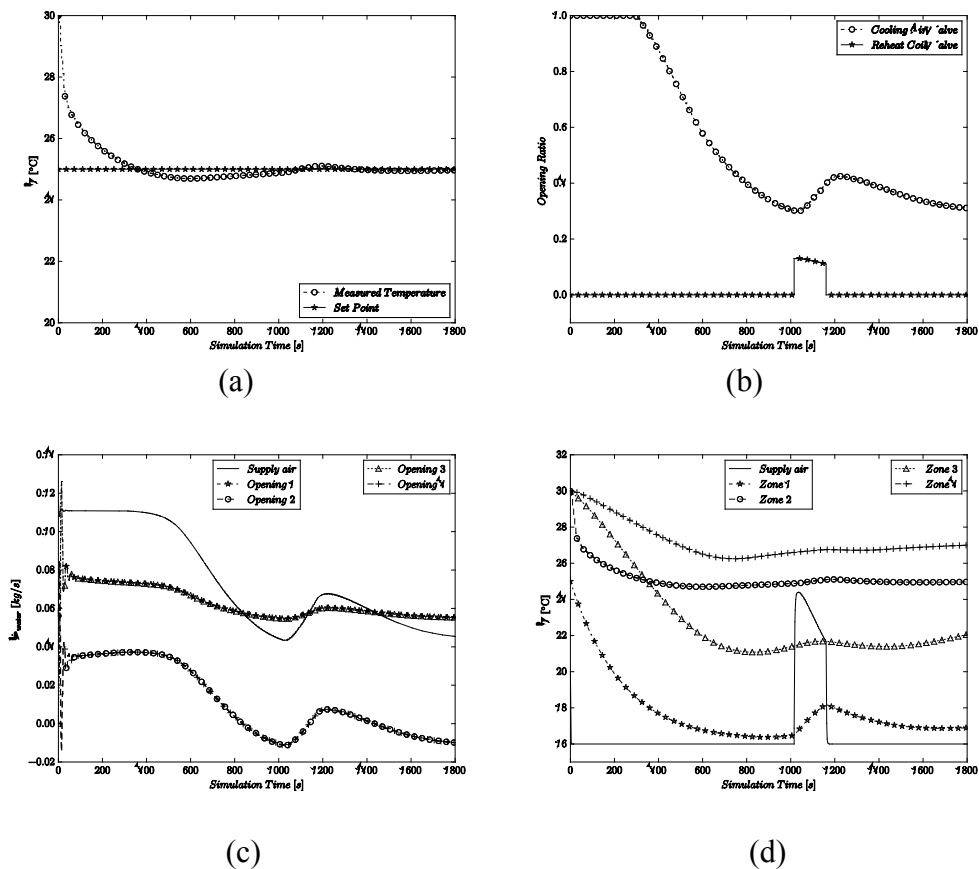


Figure 22 (a) Zone 2 temperature control; (b) Control outputs from VAV terminal box; (c) Mass flow rates at different openings; (d) Zone temperature in the space

The whole mechanism in this case study is like that in section 4.3 for the dynamic changes of all the variables, except for the mass flow rate. Interestingly, at some time intervals (i.e. from 850 to 1000, from 1400 to 1800 seconds), the supply air mass flow rate is lower than the that in *Opening 1*, which resulted in the reverse flow for *Zone 3*. As such, the pressure at the outlet of *Zone 2* is larger than that at the inlet, leaving one to wonder why inflow still exists, in lieu of outflow at the inlet. The reason is that the flow in this case study is jointly determined by the inertia and buoyancy forces. During those intervals when the opening ratio of the air valve in VAV terminal box is relatively small (<0.4), the total pressure is small which indicates that buoyancy force is dominant over the momentum force. As shown in Figure 23a, there is a strong temperature stratification that is induced by the heating box. The generated buoyancy force will form the stratified pressure distribution that increases from the bottom to the top, as shown in Figure 23b. As a result, the pressure in the adjacent cells to the outlet on average are 0.57 pa while the total pressure at the outlet is 0.45 pa.

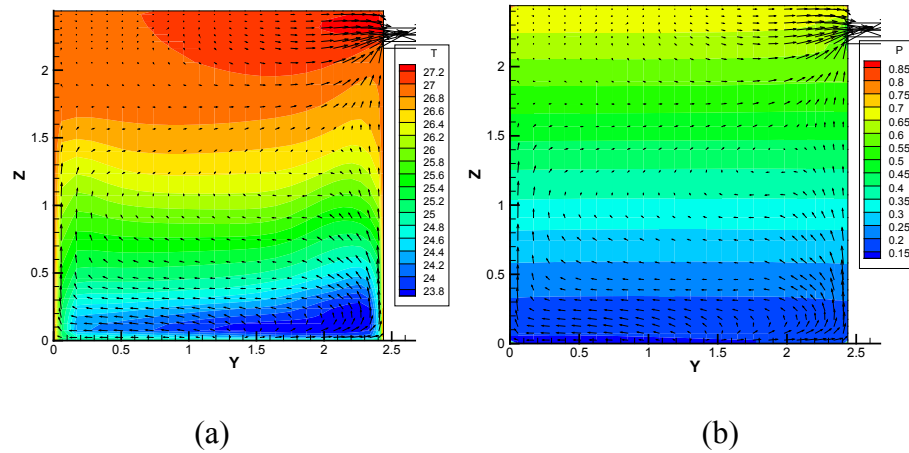


Figure 23 temperature (a) and pressure (b) distribution at plan of X=2.32 at t=1800 s

5.3 Flow with Non-Uniform Temperature Coupled to A VAV System

Based on the airflow network in section 5.2, we connected to each of 4 zones a dedicated VAV terminal box that constitutes a simplified VAV system, as shown in Figure 24. The VAV terminal boxes used here are identical to the ones in the previous sections. In this VAV system, the variable-speed fan drives the cold air of 16 °C from the air source to the terminal boxes through the pipes and splitters, and the return air gathered from the 4 zones flows back to the air sink. The fan speed is controlled by a PI controller to achieve a 140 Pa pressure difference between the supply and return ducts.

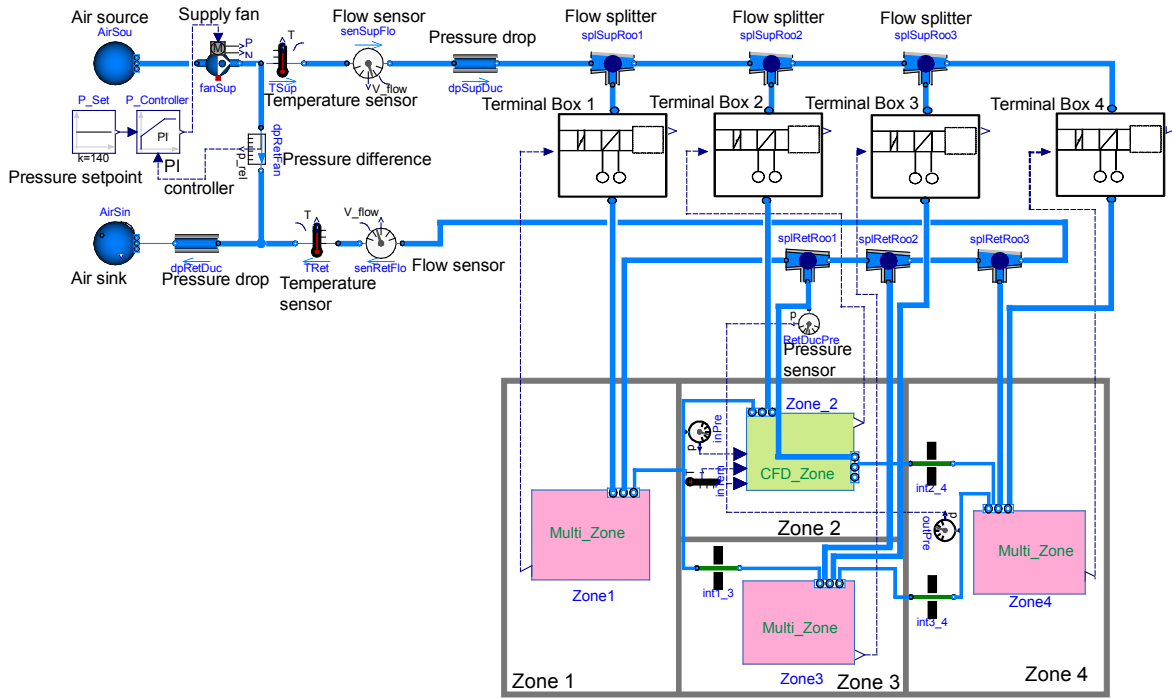


Figure 24 Sketch of VAV system connecting four zones

The inter-connection between four zones in the space is identical to that in Figure 21. Each zone has 2 additional openings to be connected to the inlet and outlet VAV terminal box. For *Zone 2*, the inlet opening and outlet opening, $0.45 \text{ m} \times 0.15 \text{ m}$, is located on the east wall and west wall, respectively. The *CFD_Zone* model is identical to that in section 4.4 while the *Multi_Zone* model is shown in Figure 25. In the center is the

Room.MixedAir model that assumes that the air in the room is uniformly mixed. Fluid ports are defined to be connected to the openings of the zones and the VAV terminal box. The room model can calculate the heat transfer between envelopes, two constant temperature models are then set to define the wall surface temperature.

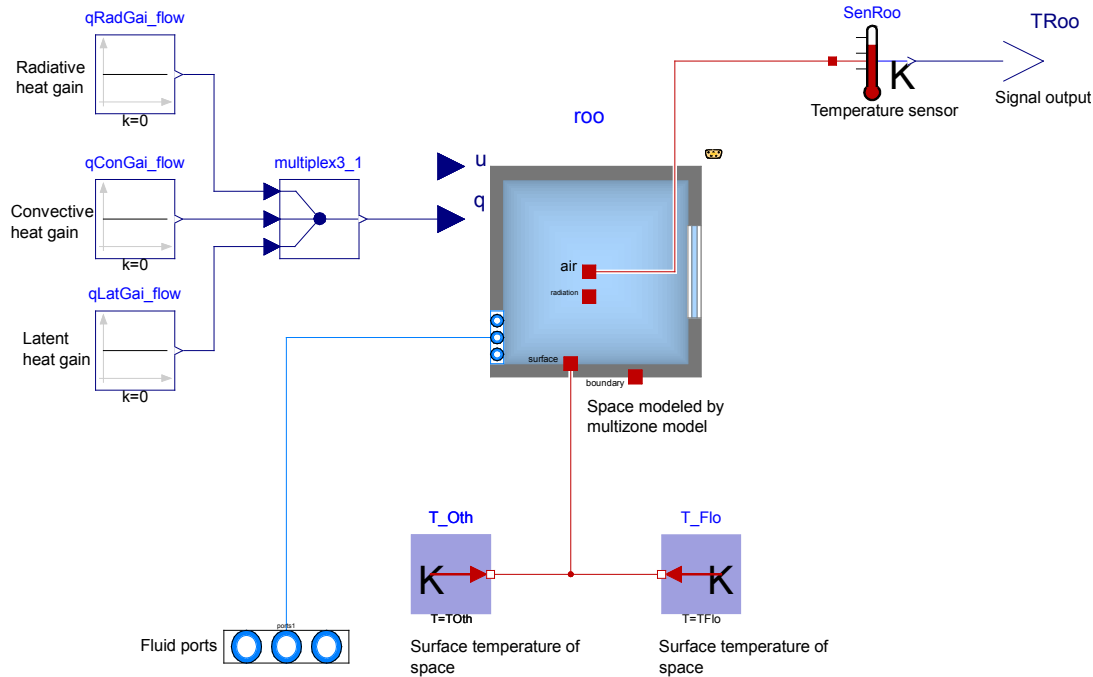


Figure 25 Sketch of multizone model

To mimic an office area, we defined the nominal mass flow rate for the VAV system as 0.1044 kg/s, leading to about 6 air changes per hour (ACH). The temperatures of the floor and other walls for *Zone 1*, *Zone 3*, and *Zone 4* are 27 °C and 25 °C, respectively. For *Zone 2*, all the walls were set to be adiabatic, as a heat source is located on the floor, which gives out a similar heat gain as other zones. The initial temperature of the air in all zones is 30 °C and the target for the VAV terminal box control is to maintain the room temperature at 25 °C.

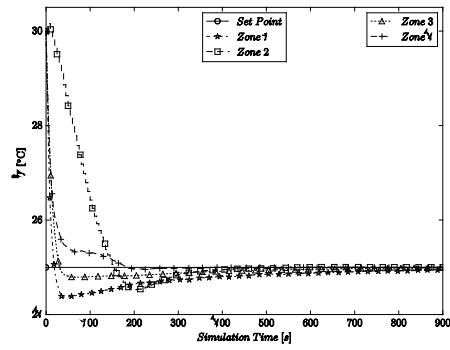
The case was simulated for 900 seconds using identical settings for the solver and tolerance as in the previous case. The dynamics of the VAV system are shown in Figure

26a-e. As the room temperature approaches the set point, the injection of cold air causes the opening of the cooling air valve in the terminal boxes to decrease gradually to 30% prior to 200 seconds, as shown in Figure 26b. Since pressure head for *terminal box 1* is the larger compared to *terminal box 3* and *terminal box 4*, we can find in Figure 26a that the speed for lowering the temperature in *Zone 1* is faster, as more cold air is injected into that zone. The decreasing speed of the valve opening for *Zone 1*, *Zone 3*, and *Zone 4* is considerably faster because the air is assumed to be instantaneously well-mixed. However, for *Zone 2* which is simulated by FFD, the decreasing speed is much slower, as it takes longer time for the stratified air to be mixed and determined. Consequently, the mass flow rate for all the terminal boxes decreases as the resistance in the branch increases significantly due to the tightening of the valve in the terminal boxes.

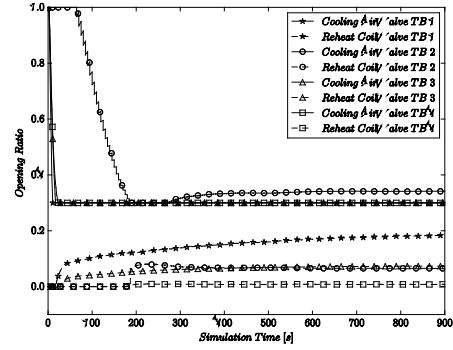
As the cooling valve opening reaches 30% and the room temperature set point is not met, the reheat in the terminal box is turned on (at 30 s for *Zone 1* and *Zone 3*; at 200 s for *Zone 2* and *Zone 4*). Accordingly, we can see in Figure 26d that the supply air temperature starts increasing instantly after the reheat coil is on. For *Zone 1*, *Zone 3* and *Zone 4*, the opening of the cooling valve in the terminal boxes remains constant at 30% and the opening of the valve in the water loop increases, as the actual temperature is lower than set point. However, for *Zone 2*, the opening of the cooling air valve increases a bit to 34% after reaching the lowest point.

Eventually, as the actual room temperature reaches the set point, the reheat for all terminal boxes remains on, because the heat gain in the zone is relatively small. As shown in Figure 26e, the pressure difference at the supply and return duct reach the set point of 140 Pa from 20 Pa, after decreasing the mass flow rate from 0.104 kg/s to 0.780 kg/s. At

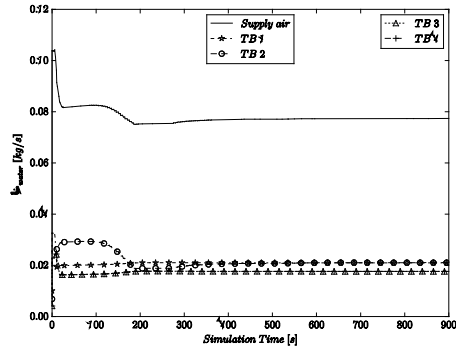
the beginning of the simulation when the duct resistance is small (cooling air valve opening is large) the supply mass flow rate of the fan is relatively large, and when the duct resistance increases (cooling air valve opening is small) as simulation progresses, the mass flow rate decreases. This is due to the operational point of the fan being fully coupled with the duct system.



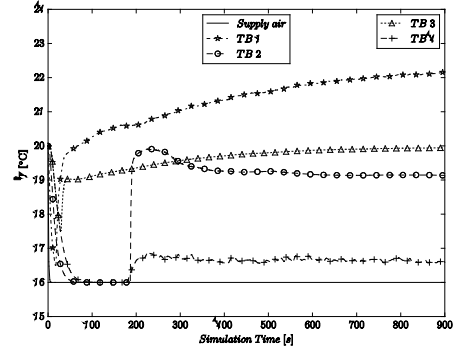
(a)



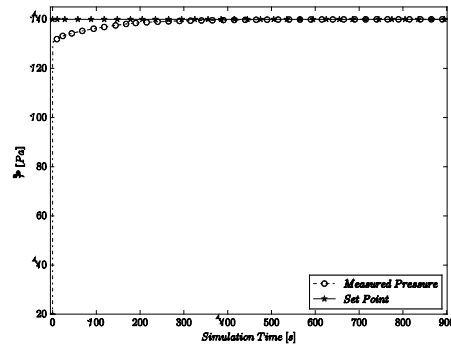
(b)



(c)



(d)



(e)

Figure 26 (a) Temperature in all zones; (b) Control outputs from VAV terminal boxes; (c) Mass flow rates supplied by VAV terminal boxes; (d) Supply temperature by VAV terminal boxes; (e) Pressure difference at supply and return duct

6 Conclusion

This paper presented coupling FFD with multizone models in the Modelica *Buildings* library to study the dynamic response of HVAC systems in large spaces with stratified airflow distributions. The quasi-dynamic data synchronization strategy was used to fulfill the exchange of information for two scenarios. The first one is a simplified scheme in which FFD calculates the mass flow rate at outlets to feed to the multizone models. The other is more sophisticated as the multizone model gives a total pressure at fluid ports to FFD and FFD then returns the mass flow rates to the multizone model.

After implementing the two coupled simulation frameworks, we demonstrated its capability by studying two cases with either non-uniform momentum or non-uniform temperature distributions. The comparison between the simulated results and experimental data showed that the coupled models are able to capture the physics associated with the non-uniformity of a dynamic system. Further by linking the flows with a VAV terminal box and a VAV system, the coupled simulation models can capture dynamics that are critical to the design and operation of the system.

In the future, the FFD simulation can be performed in parallel (Tian, Sevilla, and Zuo 2017) or a reduced order model such as in situ adaptive tabulation (Li et al. 2016; Tian, Sevilla, Li, et al. 2017) can be further used to accelerate the computation speed. With much faster simulation of the non-uniform airflow distribution, using the coupled simulation model for model-based control can be applicable.

ACKNOWLEDGMENTS

This research was supported by the National Science Foundation under Award No. IIS-1633338 and the U.S. Department of Energy under Contract No. DE-EE0007688.

This research was also supported in part by the U.S. Defense Threat Reduction Agency. LBNL's research was performed under U.S. Department of Energy Contract No. DE-AC02-05CH11231.

References

- Axley, J. 2007. Multizone Airflow Modeling in Buildings: History and Theory. *HVAC&R Research*, 13 (6):907-28.
- Beausoleil-Morrison, I. 2000. *The Adaptive Coupling of Heat and Air Flow Modelling within Dynamic Whole-Building Simulation*: Citeseer.
- Birdsall, B. E., W. F. Buhl, R. B. Curtis, A. E. Erdem, J. H. Eto, J. J. Hirsch, K. H. Olson, and F. C. Winkelmann. 1985. "The Doe-2 Computer Program for Thermal Simulation of Buildings." In *Energy Sources: Conservation and Renewables*, edited by David Hafmeister. American Institute of Physics.
- Bonvini, M., M. Popovac, and A. Leva. 2014. Sub-Zonal Computational Fluid Dynamics in an Object-Oriented Modelling Framework. *Proceedings of the Building Simulation*.
- Chen, Q., and W. Xu. 1998. A Zero-Equation Turbulence Model for Indoor Airflow Simulation. *Energy and Buildings*, 28 (2):137-44.
- Chorin, A. J. 1967. A Numerical Method for Solving Incompressible Viscous Flow Problems. *Journal of Computational Physics*, 2 (1):12-26.
- Clarke, J. A. 2001. *Energy Simulation in Building Design*: Routledge.
- Courant, R., E. Isaacson, and M. Rees. 1952. On the Solution of Nonlinear Hyperbolic Differential Equations by Finite Differences. *Communications on Pure and Applied Mathematics*, 5 (3):243-55.
- Crawley, D. B., L. K. Lawrie, C. O. Pedersen, and F. C. Winkelmann. 2000. Energyplus: Energy Simulation Program. *ASHRAE Journal* 42 (4):49-56.
- Dols, W. S., and G. N. Walton. 2002. *Contamw 2.0 User Manual: Multizone Airflow and Contaminant Transport Analysis Software*: US Department of Commerce, Technology Administration, National Institute of Standards and Technology.
- Fritzson, P. 1998. Modelica - a Language for Equation-Based Physical Modeling and High Performance Simulation. *Applied Parallel Computing*, 1541:149-60.
- Gao, Y. 2002. Coupling of Computational Fluid Dynamics and a Multizone Airflow Analysis Program for Indoor Environmental Design. *Cambridge, MA., Massachusetts Institute of Technology*.
- Jin, M., W. Zuo, and Q. Chen. 2012. Improvements of Fast Fluid Dynamics for Simulating Air Flow in Buildings. *Numerical Heat Transfer, Part B: Fundamentals*, 62 (6):419-38.

- Klein, S. A., J. A. Duffie, and W. A. Beckman. 1976. Trnsys-a Transient Simulation Program. *Ashrae Transactions*, 82:623.
- Ladeinde, F., and M. D. Nearon. 1997. CFD Applications in the HVAC&R Industry. *ASHRAE Journal*, 39 (1):44-8.
- Li, D., W. Tian, Z. Wetter, Wangda, and Michael. 2016. Simulation Using in Situ Adaptive Tabulation and Fast Fluid Dynamics. *IBPSA-USA Journal*, 6 (1).
- Liu, G., J. Zhang, and A. Dasu. 2012. Review of Literature on Terminal Box Control, Occupancy Sensing Technology and Multi-Zone Demand Control Ventilation (Dcv). *US Department of Energy, Tech. Rep.*
- Nguyen, A.-T., S. Reiter, and P. Rigo. 2014. A Review on Simulation-Based Optimization Methods Applied to Building Performance Analysis. *Applied Energy*, 113:1043-58.
- Norrefeldt, V., G. Grün, and K. Sedlbauer. 2012. Vepzo–Velocity Propagating Zonal Model for the Estimation of the Airflow Pattern and Temperature Distribution in a Confined Space. *Building and Environment*, 48:183-94.
- Nouidui, T., K. Phalak, W. Zuo, and M. Wetter. 2012. Validation and Application of the Room Model of the Modelica Buildings Library. *Proceedings of the the 9th International Modelica Conference*, Munich, Germany, September 3-5.
- Nouidui, T., M. Wetter, and W. Zuo. 2012. Validation of the Window and the Room Models of the Modelica Buildings Library. *Proceedings of the the 5th National Conference of International Building Performance Simulation Association -USA (SimBuild2012)*, Madison, WI, August 1-3.
- Srebric, J., J. Yuan, and A. Novoselac. 2008. On-Site Experimental Validation of a Coupled Multizone and CFD Model for Building Contaminant Transport Simulations. *Ashrae Transactions*, 114 (1):273-81.
- Tan, G., and L. R. Glicksman. 2005. Application of Integrating Multi-Zone Model with CFD Simulation to Natural Ventilation Prediction. *Energy and Buildings*, 37 (10):1049-57.
- Tian, W., A. T. Sevilla, D. Li, W. Zuo, and M. Wetter. 2017. Fast and Self-Learning Indoor Airflow Simulation Based on in Situ Adaptive Tabulation. *Journal of Building Performance Simulation*.
- Tian, W., T. A. Sevilla, and W. Zuo. 2017. A Systematic Evaluation of Accelerating Indoor Airflow Simulations Using Cross-Platform Parallel Computing. *Journal of Building Performance Simulation*, 10 (3):243-55. doi: 10.1080/19401493.2016.1212933.
- Tian, W., and W. Zuo. 2013. Literature Review and Research Needs to Couple Building Energy and Airflow Simulation. *Proceedings of the Proceedings of the the APEC Conference on Low-carbon Towns and Physical Energy Storage*.
- Walton, G. N. 1994. "Contam93 User Manual." In.: National Inst. of Standards and Technology (BFR), Gaithersburg, MD (United States).
- Wang, L., and Q. Chen. 2005. On Solution Characteristics of Coupling of Multizone and CFD Programs in Building Air Distribution Simulation. *Proceedings of the 9th International IBPSA Conference, Montréal*.
- Wang, L., and Q. Chen. 2007. Validation of a Coupled Multizone-CFD Program for Building Airflow and Contaminant Transport Simulations. *HVAC&R Research*, 13 (2):267-81.
- Wang, L. L., and Q. Chen. 2008. Evaluation of Some Assumptions Used in Multizone Airflow Network Models. *Building and Environment*, 43 (10):1671-7.

- Wetter, M. 2006. Multizone Airflow Model in Modelica. *Proceedings of the the 5th International Modelica Conference*, Vienna, Austria.
- Wetter, M., M. Bonvini, T. Noudui, W. Tian, and W. Zuo. 2015. Modelica Buildings Library 2.0. *Proceedings of the Abstract submitted to Building Simulation 2015*, Hyderabad, India.
- Wetter, M., and C. Haugstetter. 2006a. Modelica Versus Trnsys—a Comparison between an Equation-Based and a Procedural Modeling Language for Building Energy Simulation. *Proceedings of the Proc. of the SimBuild, 2nd National Conference of IBPSAUSA*.
- Wetter, M., and C. Haugstetter. 2006b. Modelica Versus Trnsys - a Comparison between an Equation-Based and a Procedural Modeling Language for Building Energy Simulation. *Proceedings of the the SimBuild, 2nd National Conference of IBPSA-USA*, Cambridge, MA.
- Wetter, M., W. Zuo, T. S. Noudui, and X. Pang. 2014. Modelica Buildings Library. *Journal of Building Performance Simulation*, 7 (4):253-70.
- Yang, P. 2013. "Real-Time Building Airflow Simulation Aided by GPU and FFD." Concordia University.
- Yuan, J. 2003. "Effective Prediction of Air Distribution and Contaminant Transport in Entire Buildings by Coupling Multi-Zone, CFD and Energy Models." Master's thesis, The Pennsylvania State University.
- Zhai, Z., Q. Chen, P. Haves, and J. Klems. 2002. On Approaches to Couple Energy Simulation and Computational Fluid Dynamics Programs. *Building and Environment*, 37 (8-9):857-64.
- Zuo, W., and Q. Chen. 2009. Real-Time or Faster-Than-Real-Time Simulation of Airflow in Buildings. *Indoor Air*, 19 (1):33-44.
- Zuo, W., and Q. Chen. 2010. Fast and Informative Flow Simulations in a Building by Using Fast Fluid Dynamics Model on Graphics Processing Unit. *Building and Environment*, 45 (3):747-57.
- Zuo, W., M. Jin, and Q. Chen. 2012. Reduction of Numerical Diffusion in FFD Model. *Engineering Applications of Computational Fluid Mechanics*, 6 (2):234-47.
- Zuo, W., M. Wetter, D. Li, M. Jin, W. Tian, and Q. Chen. 2014. Coupled Simulation of Indoor Environment, HVAC and Control System by Using Fast Fluid Dynamics and Modelica. *Proceedings of the 2014 ASHRAE/IBPSA-USA Building Simulation Conference*, Atlanta, GA, Sep. 10-12.
- Zuo, W., M. Wetter, W. Tian, D. Li, M. Jin, and Q. Chen. 2016. Coupling Indoor Airflow, HVAC, Control and Building Envelope Heat Transfer in the Modelica Buildings Library. *Journal of Building Performance Simulation*, 9 (4):366-81.